SIMPler realisation of Scalar Dark Matter

Preprint · April 2019

DOI: 10.48550/arXiv.1904.07562

3 authors:

Subhaditya Bhattacharya
Indian Institute of Technology Guwahati
112 PUBLICATIONS **1,879** CITATIONS
SEE PROFILE

Purusottam Ghosh
IACS
54 PUBLICATIONS **725** CITATIONS
SEE PROFILE

Shivam Verma
Ramakrishna Mission Vivekananda Educational and Research Institute
8 PUBLICATIONS **37** CITATIONS
SEE PROFILE

SIMPler realisation of Scalar Dark Matter

Subhaditya Bhattacharya, Purusottam Ghosh, Shivam Verma

Department of Physics, Indian Institute of Technology Guwahati
Guwahati, Assam 781039, India

E-mail: subhab@iitg.ac.in, pghoshiitg@gmail.com, shivam.59910103@gmail.com

Abstract. With growing agony of not finding a dark matter (DM) particle in direct search experiments so far (for example in XENON1T), frameworks where the freeze-out of DM is driven by number changing processes within the dark sector itself and do not contribute to direct search, like Strongly Interacting Massive Particle (SIMP) are gaining more attention. In this analysis, we ideate a simple scalar DM framework stabilised by Z_3 symmetry to serve with a SIMP-like DM (χ) with additional light scalar mediation (ϕ) to enhance DM self interaction. We identify that a large parameter space for such DM is available from correct relic density and self interaction constraints coming from Bullet or Abell cluster data. We derive an approximate analytic solution for freeze-out of the SIMP like DM in Boltzmann Equation describing $3 \to 2$ number changing process within the dark sector. We also provide a comparative analysis of the SIMP like solution with the Weakly Interacting Massive Particle (WIMP) realisation of the same model framework here.

Keywords: SIMP Dark Matter

Contents

1 Introduction

Numerous experimental observations at wide range of length scales [1–3], have indicated that about 80% of total matter density is dominated by Dark matter (DM) [4, 5], although we know very little about it. The absence of a particle of its kind within the Standard Model (SM), also provides a very strong motivation for the existence of physics beyond the Standard Model. Efforts are therefore being made to characterise the nature of DM and discover them in experiments. We know of it's existence through gravitational interaction, but as it doesn't interact with the electromagnetic radiations, its quite hard to detect them. There are three popular ways to detect DM through Direct search [6, 7], Indirect search [8] and Collider search experiment for example, at Large Hadron Collider (LHC) [9]. After searching for more than a decade and not being able to know much about it, puts a constraint on its properties, particularly on its coupling to the visible sector.

Amongst theoretical efforts to construct a viable DM candidate, Weakly Interacting Massive Particle (WIMPs) [10] in extensions of SM turns out to be most popular. In such a case, the DM is assumed to freeze-out from the equilibrium via $2 \to 2$ annihilations to SM and easily satisfies the relic density $\Omega h^2 \simeq 0.12$ (as indicated by PLANCK data [11]), if the DM-SM interaction is of the order of weak interaction strength. The problem with the WIMP like solution is that the same interaction also provides direct search and collider production. Therefore it is difficult to explain the non-observation of the DM in these experiments while addressing correct relic density. Alternate possibilities within the WIMP paradigm is therefore to decouple the number changing processes for freeze-out from direct search graphs through co-annihilation, semi-annihilation or DM-DM conversion (see for example, in [12, 13]).

Strongly Interacting Massive Particle (SIMP) provides an interesting alternative to predict the freeze out through number changing process within the dark sector itself through for example, $3 \to 2$ or $4 \to 2$ process. Evidently, for these processes to contribute significantly, one assumes very small $2 \to 2$ annihilation to SM aka very small DM-SM interaction and therefore has a natural explanation of non-observation of DM in direct and collider searches. DM in such a framework typically has a sub-GeV mass and a large self-scattering cross section, unlike the WIMP case [14]. Then, although such a large self-scattering cross section is constrained by Bullet cluster [15] and spherical halo shapes, it can lead to distinct signatures in galaxies and galaxy clusters, such as the offset of the dark matter sub halo from the galaxy centre, as hinted in Abell 3827 [16]. Recently in [14] it was shown that if we consider a paradigm where DM particles have a strong number changing self interaction, then the required thermal relic density parameter can be met along with addressing the problems like core vs cusp [17] and too big to fail [18] that poses a conundrum to face.

The aim of the paper is to ideate a simple dark sector that inherits the above SIMP-like credentials. The models that have been analysed so far consists of scalar DM and have an additional $U(1)$ gauge symmetry to aid self interaction through additional vector boson mediation and the remnant symmetry (after symmetry breaking) stabilizes the DM [19]. We propose a dark sector consisting of one complex scalar singlet field χ and a real scalar singlet ϕ, where χ transforms under an unbroken Z_3 symmetry and serves as DM. The scalar field ϕ is considered even under Z_3, acquires a vacuum expectation value (vev) during spontaneous symmetry breaking (SSB) and mixes with the scalar doublet to predict an additional light scalar in the theory to aid DM self interaction. We perform a detailed analysis of the relic density of the DM for freeze-out through $3 \to 2$ number changing process in the dark sector. This is possible if we assume the Higgs portal DM-SM coupling to be small. We also find out that the relic density allowed parameter space is highly constrained by the self scattering cross-section from Bullet or Abell cluster data. As the same model serves as WIMP DM with non vanishing Higgs portal coupling, we compare the outcome of SIMP like framework to the WIMP paradigm of the model.

We also make a thorough review of the Boltzman Equation describing a SIMP like solution in a model independent way and obtain an approximate analytical solution for that. The solution serves well in a range of DM mass which is validated by comparing to the numerical solution of the Boltzmann Equation.

The paper is organised as follows. We discuss the thermal freeze out for SIMP like DM in Section 2. The model construct and its relic density outcome together with the self scattering cross-section constraints are discussed in Section 3. The WIMP like solution of the model is discussed in Section 4 and then we finally conclude in Section 5. The detailed

calculation of DM annihilation cross-section to DM and to SM (both $3 \to 2$ and $2 \to 2$) and the scattering cross-section of DM with DM and SM are explicitly demonstrated in Appendix.

2 Thermal freeze out of Dark Matter in SIMP framework

In this section, we review the thermal freeze out of DM governed by Boltzmann Equation(s) (BEQ). In order for achieving a correct formalism for relic density of DM governed by the number changing process within the dark sector itself (for example, we focus on $3_{DM} \to 2_{DM}$ process in this paper, elaborated later with a specific model), we will try to identify an approximate analytical solution for the corresponding BEQ. Now, we start with a quick recap of thermal freeze-out of DM governed by $2 \to 2$ annihilation to SM particles, well known to yield a WIMP like solution, for the purpose of comparison and to use the procedure further to achieve the approximate analytical solution for SIMP framework advocated here.

2.1 A quick recap of thermal freeze-out in WIMP scenario

The very idea of thermal freeze-out of DM is based on the assumption that the DM was in thermal and chemical equilibrium in early universe. As the universe expands with Hubble rate ($\mathcal{H}$), at a particular epoch the interaction rate of the DM (Γ) falls below the rate of expansion ($\mathcal{H}$) [10] i.e.

$$\mathcal{H}\,(\text{Hubble expansion rate}) \;>\; \Gamma\,(\text{particle interaction rate}), \tag{2.1}$$

and the DM freezes out from thermal equilibrium to yield relic density. A successful DM model must yield relic density as observed in Cosmic Microwave Background (CMB) data for example, given by PLANCK [11]:

$$0.1177 \;\leq \Omega_{\rm DM} h^2 \leq\; 0.1221, \tag{2.2}$$

where $\Omega_{\rm DM} = \rho_{DM}/\rho_c$ is the cosmological DM density scaled with respect to critical density $\rho_c = 3\mathcal{H}^2/(8\pi G_N)$, with G_N denoting Newton's gravitational constant [10]. The phenomena of freeze-out or thermal decoupling happens when the temperature of the thermal bath falls (roughly) below the mass of the DM particle. The number density of the DM after freeze-out depends on its interaction rate (Γ), which in turn depends on DM mass and coupling(s) to the visible sector when the depletion in DM number density occurs via annihilation to SM particles. The BEQ that describes the thermal freeze-out of a DM species, is described in terms of the time evolution of the DM phase space distribution $f(\mathbf{r}, \mathbf{p}, t)$ through [10]:

$$\hat{\mathcal{L}}[f] = \hat{\mathcal{C}}(f), \tag{2.3}$$

where $\hat{\mathcal{L}}[f]$ is the Lioville operator describing the change in f with time, while $\hat{\mathcal{C}}(f)$ denotes the change in f through collision. Left hand side of the above equation remains unchanged in a homogeneous and isotropic universe (governed by Friedman-Robertson-Walker metric)[1], while different possibilities of DM collision term $\hat{\mathcal{C}}(f)$ can yield different possibilities of DM freeze-out and relic density, as we elaborate here. The simplest realisation for the collision term $\hat{\mathcal{C}}(f)$ is obtained when two DM particles annihilate to two SM particles following the cartoon in Fig. 1. This is a standard number changing process for DM to yield WIMP like solution, which dictates that DM better have annihilation cross-section of the strength of

[1] which also dictates $f(\mathbf{r}, \mathbf{p}, t) \to f(E, t)$.

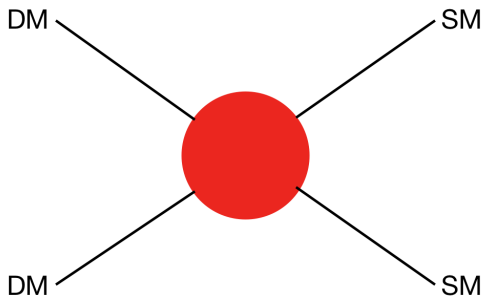

Figure 1: A cartoon of two DM particles annihilating to two SM particles to yield a WIMP-like scenario.

weak interactions to justify the observed relic density. The BEQ describing such $2_{DM} \to 2_{SM}$ process can be written in terms of DM number density $n = (g/(2\pi)^3) \int d^3p\ f(E,t)$ as [10]:

$$\begin{aligned}\frac{dn}{dt} + 3Hn &= \int \frac{g_{DM}\ d^3p_1}{(2\pi)^3 2E_1} \frac{g_{DM}\ d^3p_2}{(2\pi)^3 2E_2} \frac{g_{SM}\ d^3p_3}{(2\pi)^3 2E_3} \frac{g_{SM}\ d^3p_4}{(2\pi)^3 2E_4} (2\pi)^4 \delta^4(p_1 + p_2 - p_3 - p_4) \\ &\qquad \times |\mathcal{M}_{1+2\to 3+4}|^2 \ \ (f_{DM} f_{DM} - f^{eq}_{DM} f^{eq}_{DM}) \\ &= -\langle \sigma v \rangle_{2\to 2} \Big[n^2 - (n_{eq})^2 \Big] \ , \end{aligned} \tag{2.4}$$

where $f^{eq} = e^{-E/T}$ and $\langle \sigma v \rangle_{2_{DM}\to 2_{SM}}$ is the thermal average annihilation cross-section given by [10, 20, 21],

$$\begin{aligned}\langle \sigma v \rangle_{2_{DM}\to 2_{SM}} &= \frac{1}{n_1^{eq}\ n_2^{eq}} \int \frac{g_{DM}\ d^3p_1}{(2\pi)^3 2E_1} \frac{g_{DM}\ d^3p_2}{(2\pi)^3 2E_2} \frac{g_{SM}\ d^3p_3}{(2\pi)^3 2E_3} \frac{g_{SM}\ d^3p_4}{(2\pi)^3 2E_4} (2\pi)^4 \delta^4(p_1 + p_2 - p_3 - p_4) \\ &\qquad \times |\mathcal{M}_{1+2\to 3+4}|^2\ f_1^{eq}\ f_2^{eq} \qquad . \\ &= \int_{4m^2_{DM}}^{\infty} ds \frac{s\sqrt{(s - 4m^2_{DM})}\ K_1(\sqrt{s}/T)\ (\sigma v)_{2_{DM}\to 2_{SM}}}{16T\ m^4_{DM}\ [K_2(m_{DM}/T)]^2} \end{aligned} \tag{2.5}$$

g_{DM} denotes internal degrees of freedom of DM particles, and g_{SM} denote internal degrees of freedom of SM particles. One can further parameterize this equation by substituting the number density per co-moving volume: $Y = n/s$, where s is the entropy density and $x = m_{DM}/T$ to yield [10]:

$$\frac{dY}{dx} = -0.264\ g_*^{1/2}\ M_{pl} \frac{m_{DM}}{x^2}\ \langle \sigma v \rangle_{2\to 2} \left(Y^2 - (Y_{eq})^2 \right) . \tag{2.6}$$

Using Maxwell-Boltzmann statistics for both fermions and Bosons in non-relativistic regime, the equilibrium number density per co moving volume turns out [10]:

$$Y_{eq}(x) = 0.145\ \frac{g_{DM}}{g_*} x^{3/2} e^{-x} \ , \tag{2.7}$$

g_* denotes the relativistic degrees of freedom (SM particles), for GeV order DM $g_* = 106.75$. With all these inputs, one can now solve the BEQ 2.6 numerically to obtain freeze out of

DM and present yield after freeze out, which is $Y(x \to \infty)$. Using $n_{DM} = sY(x \to \infty)$, one can find relic density of DM as [10]:

$$\Omega h^2 = 2.752 \times 10^8 \left(\frac{m_{DM}}{\text{GeV}}\right) Y(x \to \infty) \ . \tag{2.8}$$

One can also estimate $Y(x \to \infty)$ approximately without solving BEQ numerically (Eq:2.6) and relic density of DM can be expressed in terms of annihilation cross-section $\langle\sigma v\rangle_{2_{DM}\to 2_{SM}}$ (see for example, [10]):

$$\Omega h^2 \approx \frac{854.45 \times 10^{-13}}{\sqrt{g_*}} \ x_f \left(\frac{\text{GeV}^{-2}}{\langle\sigma v\rangle_{2\to 2}}\right) , \tag{2.9}$$

where x_f correspond to freeze-out temperature of DM that is given by [10]:

$$\begin{aligned} x_f \approx \ln\Big[0.038 \ \frac{g_{DM}}{\sqrt{g_*}} \ M_{Pl} \ m_{DM} \ (c+2)c \ \langle\sigma v\rangle_{2\to 2}\Big] \\ - \frac{1}{2} \ln\ln\Big[0.038 \ \frac{g_{DM}}{\sqrt{g_*}} \ M_{Pl} \ m_{DM} \ (c+2)c \ \langle\sigma v\rangle_{2\to 2}\Big]. \end{aligned} \tag{2.10}$$

In the above equation, at $x = x_f$, $\Delta(x_f) = cY_{eq}(x_f)$ where c is an unknown constant and $\Delta = Y - Y_{eq}$. An example of DM freeze-out in WIMP-like scenario is shown in the right hand side (RHS) of Fig. 3 for a DM mass of 100 GeV with different possible values of annihilation cross-section $\langle\sigma v\rangle_{2_{DM}\to 2_{SM}}$ in $Y-x$ plane. The correct relic density $\Omega_{DM}h^2 \sim 0.12$ line is also shown so that $\langle\sigma v\rangle_{2_{DM}\to 2_{SM}} \sim 1.5 \times 10^{-8}$ GeV^{-2}, typical cross-section of weak interaction scale matches to it. We will now follow the same procedure to find out the freeze-out through the SIMP mechanism.

2.2 SIMP scenario

Let us now turn to the SIMP realization of DM freeze out. SIMP mechanism can be achieved when $2 \to 2$ annihilation to SM is suppressed and change in DM number density is mainly dictated within dark sector for example, by $3_{DM} \to 2_{DM}$ process. Given the fact that the DM has still to be in equilibrium in the early universe, the $2 \to 2$ interaction with SM can not be completely neglected. Actually, the scattering with the SM via the same $2_{DM} \to 2_{SM}$ interaction can still be sizeable enough even if the annihilation cross section is low due to the large SM number density. This helps the DM to keep up with equilibrium while not heating up the dark sector until the DM freezes out, following the inequality condition [14]:

$$\Gamma_{2\to 2 \ \text{ scattering}} \gtrsim \Gamma_{3\to 2 \ \text{ annihilation}} \gg \Gamma_{2\to 2 \ \text{ annihilation}} \ . \tag{2.11}$$

In above equation, $\Gamma_{2\to 2 \ \text{ scattering}} = n^{eq}\langle\sigma v\rangle$, $\Gamma_{2\to 2 \ \text{ annihilation}} = n_{DM}\langle\sigma v\rangle$ and $\Gamma_{3\to 2} = n_{DM}\langle\sigma v^2\rangle$ defines the strength of the corresponding interactions. We will put up an explicit demonstration of the inequality Eq. 2.11 in context of the model described here later. The scattering does not contribute to the relic density of the DM caveat to a kinetic decoupling (see for example, the discussion on ELDER DM as in [22]); therefore the number changing processes that govern the freeze-out for SIMP type framework can be described by Fig. 2, where the sizes of the diagrams ($3_{DM} \to 2_{DM}$ versus $2_{DM} \to 2_{SM}$ annihilation) roughly indicate the dominant and sub-dominant contributions.

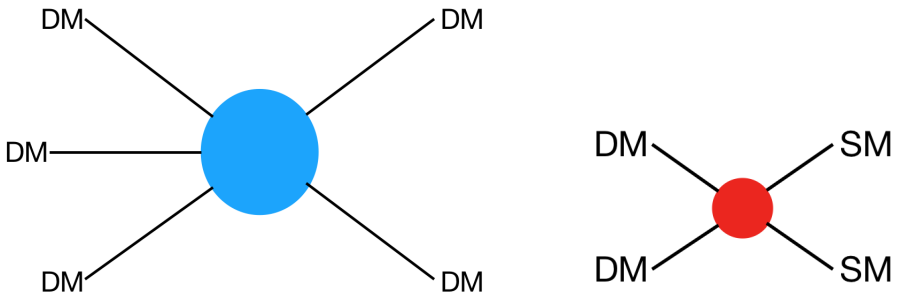

(a) (b)

Figure 2: A cartoon of annihilation process of three DM particles to two DM particles in SIMP scenario assisted with $2 \to 2$ annihilation to SM particles. The sizes of the diagrams roughly indicate the strengths of the processes (not in exact scale).

Mass dimension of thermally averaged cross section for a general $n \to 2$ annihilation processes, where n is the initial number of DM particle and 2 corresponds to the number of particles in the final state [23]:

$$[< \sigma_{n\to 2} v^{n-1} >] = [M^{-3n+4}]. \tag{2.12}$$

According to Eq. 2.12, a $2 \to 2$ process is: $[\langle\sigma v\rangle] = [M]^{-2}$, with unit GeV^{-2} (assuming the mass of the DM $\sim$ GeV and 'v' to be dimensionless in natural units). Similarly for a $3 \to 2$ process, $[\langle\sigma v^2\rangle] = [M]^{-5}$, so it has unit GeV^{-5}. In the following subsection, we discuss the Boltzmann equation for $3_{DM} \to 2_{DM}$ number changing process and its possible analytical solutions for freeze-out.

2.2.1 Boltzmann Equation and numerical solution to freeze-out

The Boltzmann Equation (BEQ) that dictates the freeze-out through $3_{DM} \to 2_{DM}$ number changing process in dark sector (see Fig. 2a only), in terms of DM number density, n [2] [10, 24]

$$\begin{aligned}\frac{dn}{dt} + 3Hn = &\int \frac{g_{DM}\, d^3p_1}{(2\pi)^3 2E_1}\frac{g_{DM}\, d^3p_2}{(2\pi)^3 2E_2}\frac{g_{DM}\, d^3p_3}{(2\pi)^3 2E_3}\frac{g_{DM}\, d^3p_4}{(2\pi)^3 2E_4}\frac{g_{DM}\, d^3p_5}{(2\pi)^3 2E_5}\,(2\pi)^4 \\ &\delta^4(p_1+p_2+p_3-p_4-p_5)|\overline{\mathcal{M}_{1+2+3\to 4+5}}|^2\;\; (f_{DM}\, f_{DM}\, f_{DM} - f^{eq}_{DM}\, f^{eq}_{DM}) \\ &= -\langle\sigma v^2\rangle_{3\to 2}\Big(n^3 - n^2 n_{eq}\Big),\end{aligned} \tag{2.13}$$

where g_{DM} denotes the internal degrees of freedom in the DM sector. The thermal average of annihilation cross section $\langle\sigma v^2\rangle_{3\to 2}$ in this case is given by [24]:

$$\begin{aligned}\langle\sigma v^2\rangle_{3\to 2} = \frac{1}{n_1^{eq}\, n_2^{eq}\, n_3^{eq}}\int &\frac{g_{DM}\, d^3p_1}{(2\pi)^3 2E_1}\frac{g_{DM}\, d^3p_2}{(2\pi)^3 2E_2}\frac{g_{DM}\, d^3p_3}{(2\pi)^3 2E_3}\frac{g_{DM}\, d^3p_4}{(2\pi)^3 2E_4}\frac{g_{DM}\, d^3p_5}{(2\pi)^3 2E_5} \\ &(2\pi)^4\delta^4(p_1+p_2+p_3-p_4-p_5)\times\overline{|\mathcal{M}_{1+2+3\to 4+5}|^2} f_1^{eq} f_2^{eq} f_3^{eq}\end{aligned} \tag{2.14}$$

In terms of co-moving number density, i.e. $Y = n/s$ and $x = m_{DM}/T$, the BEQ turns out to be [10]

$$\frac{dY}{dx} = -0.116\; g_*{}^{\frac{3}{2}} M_{Pl}\frac{{m_{DM}}^4}{x^5}\;\langle\sigma v^2\rangle_{3\to 2}\;\Big(Y^3 - Y^2\, Y_{eq}\Big). \tag{2.15}$$

[2] As argued before, the $2_{DM} \to 2_{SM}$ annihilation to SM can never be neglected, however, its contribution to DM freeze-out can be neglected in SIMP like situation as we will demonstrate later.

The equilibrium yield is $Y_{eq}(x) = 0.145\ (g_{DM}/g_*)x^{3/2}e^{-x}$, with $g_* = 10.75$ for MeV order DM. Again, one can solve the BEQ (Eq. 2.15) numerically to find the yield after freeze out: $Y(x \to \infty)$. One such numerical solution is demonstrated in the left panel of Fig. 3. The freeze-out governed by the $3_{DM} \to 2_{DM}$ process in dark sector is clearly visible from the left panel of 2a. For illustration, we have chosen the mass of the DM to be 100 MeV and different magnitudes of annihilation cross-section $\langle\sigma v^2\rangle_{3_{DM}\to 2_{DM}} \sim \{10^4 - 10^9\}\text{GeV}^{-5}$ has been shown to alter the freeze-out and relic yield. The one corresponding to correct relic density (horizontal black dashed line) is $\langle\sigma v^2\rangle_{3_{DM}\to 2_{DM}} \sim 2.5 \times 10^6\ \text{GeV}^{-5}$, that lies in the strong interaction range. This is easily contrasted to WIMP case ($2_{DM} \to 2_{SM}$) on the right panel graph, where correct relic density is obtained for 100 GeV DM with $\langle\sigma v\rangle_{2_{DM}\to 2_{SM}} \sim 1.5 \times 10^{-8}\ \text{GeV}^{-2}$. As stated earlier, relic density of DM in terms of yield after freeze out reads as [10, 21]

$$\begin{aligned} \Omega h^2 &= 2.752 \times 10^8 \left(\frac{m_{DM}}{\text{GeV}}\right) Y(x \to \infty)\ , \\ &= 2.752 \times 10^5 \left(\frac{m_{DM}}{\text{MeV}}\right) Y(x \to \infty)\ , \end{aligned} \tag{2.16}$$

where the numerical pre factor depends on the choice of DM mass in MeV or in GeV order.

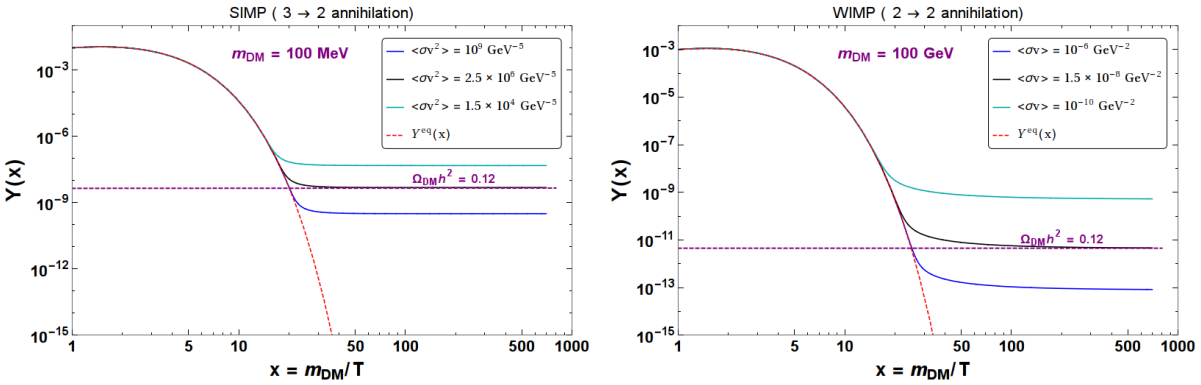

Figure 3: Freeze out of SIMP like DM($3_{DM} \to 2_{DM}$),(left panel) and WIMP like DM ($2_{DM} \to 2_{SM}$)(right panel) from equilibrium $Y^{eq}(x)$ (red dashed line) in $Y(x) - x$ plane obtained from the numerical solution of the corresponding BEQ (Eq. 2.15 and Eq. 2.6 respectively for SIMP and WIMP case). DM mass and annihilation cross-sections have been chosen in a model independent way.

2.2.2 Approximate analytical solution to Boltzmann Equation

The main idea of this section is to find an approximate analytical solution to the $3_{DM} \to 2_{DM}$ SIMP-like BEQ as in Eq. 2.15. Such an exercise has already been standardised for $2_{DM} \to 2_{SM}$ case and will be followed here. We first rewrite the BEQ (Eq. 2.15) in terms of $\Delta = Y - Y_{eq}$, that marks the difference of DM yield from the equilibrium yield. When Δ is small, the DM is in equilibrium, when Δ turns large, the DM freezes out. The BEQ in terms of Δ reads as [10]

$$\frac{d\Delta}{dx} + \frac{dY_{eq}}{dx} = -\frac{A}{x^5}\Delta\left(Y_{eq}^2 + 2\Delta Y_{eq} + \Delta^2\right)\ , \tag{2.17}$$

where we have dumped everything into $A = 0.116\ g_*^{\frac{3}{2}}\ M_{Pl}\ {m_{DM}}^4\ \langle\sigma v^2\rangle_{3_{DM}\to 2_{DM}}$. Before freeze-out, i.e. for $1 < x \leq x_f$, $\Delta << Y_{eq}$ and $d\Delta/dx \to 0$. Then BEQ simplifies to:

$$\frac{dY_{eq}}{dx} = -\frac{A}{x^5}\Delta\Big((Y_{eq})^2 + 2\Delta Y_{eq} + \Delta^2\Big)\ . \tag{2.18}$$

Near freeze-out, i.e. for $x \sim x_f$, one can assume $\Delta(x_f) = c\ Y_{eq}(x_f)$ [10] where c is an unknown constant. The BEQ turns out to be:

$$\begin{aligned}
\frac{dY_{eq}}{dx}|_{x=x_f} &= -\frac{A}{x_f^5}\Delta(x_f)\ \Big(Y_{eq}^2(x_f) + 2\Delta(x_f)\ Y_{eq}(x_f) + \Delta^2(x_f)\Big)\ , \\
\Rightarrow \Big(1 - \frac{3}{2x_f}\Big) &= \frac{A}{x_f^5}c(c+1)^2 Y_{eq}^2(x_f) \qquad \Big[\text{using } \Delta(x_f) = c\ Y_{eq}(x_f)\Big] \\
\Rightarrow \Big(1 - \frac{3}{2x_f}\Big) &= \frac{A}{x_f^5}c(c+1)^2\Big(0.145\ \frac{g_{DM}}{g_*}x_f^{3/2}e^{-x_f}\Big)^2 \quad \Big[\text{using } Y_{eq} = 0.145\ \frac{g_{DM}}{g_*}x^{3/2}e^{-x}\Big] \\
\Rightarrow \Big(x_f^2 - \frac{3}{3}x_f\Big) &= 0.0024\frac{g_{DM}^2}{\sqrt{g}_*}\ c(c+1)^2\ M_{Pl}\ m_{DM}^4\ \langle\sigma v^2\rangle_{3\to 2}\ e^{-2x_f} \qquad \Big[\text{using } A\Big] \\
\Rightarrow x_f^2 &= 0.0024\frac{g_{DM}^2}{\sqrt{g}_*}\ c(c+1)^2\ M_{Pl}\ m_{DM}^4\ \langle\sigma v^2\rangle_{3\to 2}\ e^{-2x_f}
\end{aligned} \tag{2.19}$$

One can solve for freeze-out x_f iteratively from above equation to obtain:

$$\begin{aligned}
x_f\ \approx\ & \frac{1}{2}\ln\Big[0.0024\frac{g_{DM}^2}{\sqrt{g}_*}\ c(c+1)^2\ M_{Pl}\ m_{DM}^4\ \langle\sigma v^2\rangle_{3_{DM}\to 2_{DM}}\Big] \\
& - 2\ln\Big[\frac{1}{2}\ln\Big[0.0024\frac{g_{DM}^2}{\sqrt{g}_*}\ c(c+1)^2\ M_{Pl}\ m_{DM}^4\ \langle\sigma v^2\rangle_{3_{DM}\to 2_{DM}}\Big]\Big]
\end{aligned} \tag{2.20}$$

Therefore, given the knowledge of DM mass and annihilation cross-section $\langle\sigma v^2\rangle_{3_{DM}\to 2_{DM}}$, one can find the decoupling or freeze-out temperature x_f. It is straightforward to show that for correct relic density (for example, with $m_{DM} \sim 100$ MeV and $\langle\sigma v^2\rangle_{3\to 2} \sim 2.5 \times 10^6\ \text{GeV}^{-5}$ as shown in he left panel of Fig. 3), $x_f \sim 20$, which is similar to WIMP like scenarios. This is shown in Fig. 4 for different values of the unknown constant c as a function of DM mass and we see that a large variation in c produces only a small change in x_f.

For relic density, one needs to find out the yield after freeze out. For this, we need to focus at $x >> x_f$, where $Y_{eq} \to 0$. The Eq. 2.17 simplifies to a great extent to take the

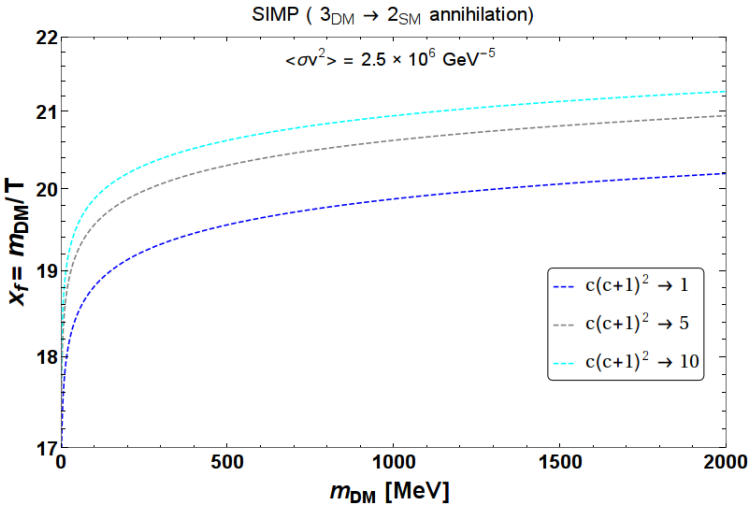

Figure 4: Variation in analytical solution of x_f as in Eq. 2.20 by choosing different values of c, where $c = \Delta(x_f)/Y_{eq}(x_f)$.

following form:

$$\frac{d\Delta}{dx} = -\frac{A}{x^5}\Delta^3 \tag{2.21}$$

$$\int_{\Delta(x_f)}^{\Delta(x\to\infty)} -\frac{d\Delta}{\Delta^3} = A\int_{x_f}^{\infty}\frac{dx}{x^5}$$

$$\Rightarrow \frac{1}{\Delta(x\to\infty)^2} - \frac{1}{\Delta(x_f)^2} = \frac{A}{2x_f^4}$$

$$\Rightarrow \frac{1}{\Delta(x\to\infty)^2} = \frac{A^2Y_{eq}^2}{x_f^{10}} + \frac{A}{2x_f^4} = \frac{A(2AY_{eq}^2 + x_f^6)}{2x_f^{10}} \quad \left[\text{from Eq.2.18, } \Delta(\mathrm{x_f}) = \frac{\mathrm{x_f^5}}{\mathrm{A\ Y_{eq}(x_f)}}\right]$$

$$\Rightarrow \Delta(x\to\infty) = \sqrt{\frac{2}{A}}\,x_f^2 \qquad \left[A\,Y_{eq}^2 << x_f^6\right]$$

$$\Rightarrow Y(x\to\infty) = \sqrt{\frac{2}{0.12 g_*^{\frac{3}{2}}\ M_{Pl}\ m_{DM}^4\ \langle\sigma v^2{}_{3_{DM}\to 2_{DM}}\rangle}}\ x_f^2\ . \tag{2.22}$$

Now From Eq. 2.16 and Eq. 2.21, one can write the expression of relic density as follows:

$$\begin{aligned}\Omega h^2 &= 2.752\times 10^8\left(\frac{m_{DM}}{MeV\times 10^3}\right)\times\sqrt{\frac{2}{0.12 g_*^{\frac{3}{2}}\ M_{Pl}\ m_{DM}^4\ \langle\sigma v^2\rangle_{3_{DM}\to 2_{DM}}}}\\ &= \frac{0.33}{g_*{}^{\frac{3}{4}}}\left(\frac{MeV\times 10^3}{m_{DM}}\right)\ x_f^2\ \left(\frac{GeV^{-5}}{\langle\sigma v^2\rangle_{3_{DM}\to 2_{DM}}}\right)\ .\end{aligned} \tag{2.23}$$

Now, we are in a position to check the reliability of the analytical solution for DM relic density obtained for the SIMP like case (Eq. 2.23) to that of the numerical solution obtained from the BEQ 2.15. This is shown in Fig. 5. We plot relic density obtained from both numerical solution and approximate analytical solution together for different values of c and for two different annihilation cross-section $\langle\sigma v^2\rangle_{3_{DM}\to 2_{DM}} = \{2\times 10^6, 10^9\}$ GeV^{-5}

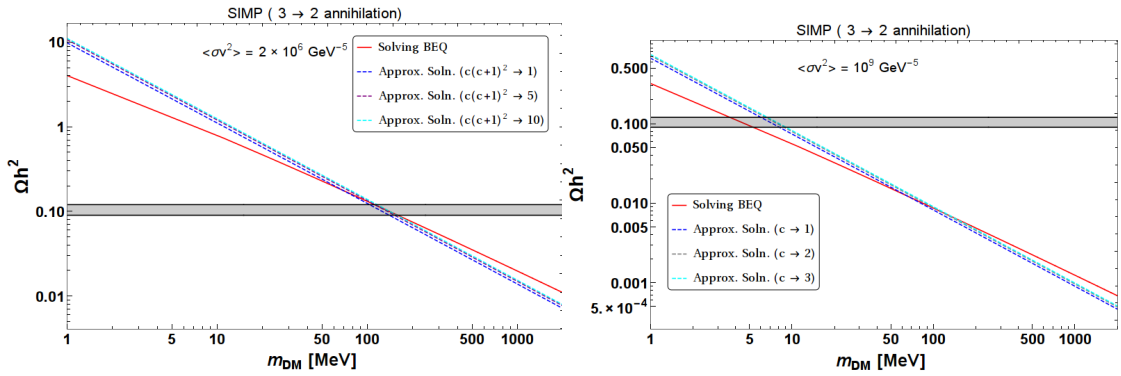

Figure 5: Comparison of relic density obtained by numerical solution to BEQ in Eq. 2.15 and that from approximate analytical solution obtained in Eq. 2.23 as a function of DM mass for different choices of c. We choose two different annihilation cross-section $\langle\sigma v^2\rangle_{3\to2} = \{2\times10^6, 10^9\}$ GeV^{-5} in left and right panel respectively. Correct relic density ($\Omega_{DM}h^2 = 0.1199 \pm 0.0022$) is indicated by the shaded band.

in left and right panel respectively. We see that the analytical solution closely mimic the numerical solution for a certain region of DM mass (50-100 MeV) and so are the corresponding annihilation cross-section $\langle\sigma v^2\rangle$. The difference rises for small and large DM masses. Actually, the cause of this discrepancy occurs when we simplify the Eq.2.17 to Eq.2.21 to only retain term of the order $\sim \Delta^3$. If we consider the second order term in $\Delta(x)$, the form of the equation looks like that of Abel equation of first kind [25], solving that will mimic the numerical solution even more closely.

3 Model specific analysis of a SIMP Framework

3.1 The Model

The idea is to identify a simple model that demonstrates SIMP criteria for freeze out of a DM as elaborated before [19, 23, 24, 26–31]. If simplicity is the guiding principle to realise a SIMP paradigm, one should focus on scalar DM (χ). The DM also need to possess an additional symmetry for stability (call it a dark symmetry) distinct from that of the SM. If we require a vertex consisting of three DM fields (χ^3) for the DM to enable a $3_{DM} \to 2_{DM}$ interaction, the minimal choice for the symmetry under which χ transforms non trivially is $\mathcal{Z}_3$. As the roots of Z_3 are complex $(1, \omega, \omega^2)$, the scalar DM χ needs to be complex. In principle, this is enough to ideate $3_{DM} \to 2_{DM}$ interactions through χ mediation itself. However, it turns out that relic density allowed parameter space for this simplest possibility is quite restrictive and even more so when we impose the self scattering (we will have explicit demonstration later) and unitarity bound data. We can enlarge the available parameter space by connecting the graph for $3_{DM} \to 2_{DM}$ process to the other end in presence of a mediator, which doesn't have $\mathcal{Z}_3$ charge. But, this can not be realised with a SM particle (even if Higgs has a portal interaction with our DM) unless we augment the SM with another additional field. Again, the minimal choice of such mediator will be another scalar ϕ (real scalar for simplicity) which is singlet under SM.

Therefore, in this model, we consider a complex scalar singlet field χ which transforms under $\mathcal{Z}_3$ and acts as DM, while under Z_3 the real scalar singlet ϕ field transforms

non-trivially. The Z_3 transformation properties of the additional scalars assumed here is mentioned in Table 1. In SIMP paradigm, the freeze out is mainly driven by $3_{DM} \to 2_{DM}$ number changing process, so the $2_{DM} \to 2_{SM}$ interaction can be killed by choosing a negligible value of the Higgs portal coupling. Now, if we provide VEV to ϕ, then it will mix with SM Higgs after spontaneous symmetry breaking and will mediate the number changing process in the dark sector. The mass of the additional scalar can be fairly light (being singlet) and will aid to annihilation cross-section providing cushion to the DM coupling to remain within perturbative limit.

Particle	**Nature**	Z_3 **transformation**
χ	Complex Scalar Singlet	ω
ϕ	Real Scalar Singlet	1
H	SM Higgs Doublet	1

Table 1: Z_3 charges of the additional scalar fields assumed in the model (χ, ϕ).

The relevant Lagrangian for this model can be mainly segregated into two parts :

$$\mathcal{L} = \mathcal{L}_{\rm SM} + \mathcal{L}_{\rm BSM}. \tag{3.1}$$

Here, we are interested in the part describing the dark sector:

$$\mathcal{L}_{\rm BSM} = \frac{1}{2}(\partial^\mu \phi)(\partial_\mu \phi) + (\partial^\mu \chi)^*(\partial_\mu \chi) - V(H, \phi, \chi). \tag{3.2}$$

The scalar potential involving the additional scalars and SM Higgs (H) reads as [14, 32]:

$$\begin{aligned} V(H,\phi,\chi) \;=\; & -\mu_H^2 H^\dagger H + \lambda_H (H^\dagger H)^2 - \frac{1}{2}\mu_\phi^2 \phi^2 + \frac{1}{4}\lambda_\phi\ \phi^4 \\ & + \frac{\mu_3}{3}\phi^3 + \frac{1}{2}\lambda_{\phi h}\ \phi^2\ H^\dagger H + \mu_{\phi h}\ \phi\ (H^\dagger H) \\ & + \mu^2 |\chi|^2 + \lambda_\chi |\chi|^4 + \frac{1}{3!}\mu_\chi(\chi^3 + \chi^{*3}) + \lambda_{\chi h}\ |\chi|^2 H^\dagger H \\ & + \frac{1}{2}\lambda_{\chi\phi}|\chi|^2\phi^2 + \mu_{\chi\phi}\ \phi\ |\chi|^2 + \frac{1}{3!}Y_{\chi\phi}\ \phi\ (\chi^3 + \chi^{*3}). \end{aligned} \tag{3.3}$$

As has already been mentioned, $3_{DM} \to 2_{DM}$ interactions are mediated by the self couplings of χ, namely involving $|\chi|^4$ and χ^3 terms. ϕ mediates additional channels through the two terms $\chi^3\phi$ and $|\chi|^2\phi^2$, when ϕ acquires a VEV. After spontaneous symmetry breaking (SSB) for this model indicates that ϕ and H mixes through their VEVs (v_ϕ and v_h) as follows:

$$\phi \to \Phi + v_\phi, \tag{3.4}$$

$$H \to \begin{pmatrix} 0 \\ \frac{h+v_h}{\sqrt{2}} \end{pmatrix}. \tag{3.5}$$

The squared mass matrix for the interaction basis, $(h\ \Phi)^T$ is given as,

$$M^2_{h\Phi} = \begin{pmatrix} 2v_h^2\lambda_h & v_h v_\phi \lambda_{\phi h} + v_h \mu_{h\phi} \\ v_h v_\phi \lambda_{\phi h} + v_h \mu_{h\phi} & \mu_3 v_\phi + 2v_\phi^2 \lambda_\phi - \mu_{h\phi}(v_h^2/2v_\phi), \end{pmatrix} = \begin{pmatrix} A & B \\ B & C \end{pmatrix}. \tag{3.6}$$

This essentially do not hamper the phenomenological outcome of this analysis. Rather, it provides an additional freedom in choosing the correct Higgs mass and mixing.

The physical scalars (h_1 and h_2) are obtained from h, Φ by choosing the following transformation,

$$\begin{pmatrix} h_1 \\ h_2 \end{pmatrix} = \begin{pmatrix} \cos\theta & -\sin\theta \\ \sin\theta & \cos\theta \end{pmatrix} \begin{pmatrix} h \\ \Phi \end{pmatrix} \tag{3.7}$$

The mass eigenvalues are therefore obtained by diagonalising the above mass matrix ($M^2_{h\Phi}$) and is given by:

$$\begin{aligned} m^2_{h_1} &= A\ \cos^2\theta + C\ \sin^2\theta - B\ \sin 2\theta \\ m^2_{h_2} &= A\ \sin^2\theta + C\ \cos^2\theta + B\ \sin 2\theta. \end{aligned} \tag{3.8}$$

The physical states are related to the flavour states through the mixing angle θ as follows:

$$\tan\ 2\theta = \frac{2B}{C - A} \tag{3.9}$$

Now, we are all set to address the phenomenology of the scalar sector. Let h_2 be the SM like Higgs ($m_{h_2} = 125$ GeV and $v_h = 246$ GeV) and h_1 be the additional scalar boson. The additional scalar being a singlet predominantly, can be heavier or lighter than the SM Higgs, because it can't be produced at colliders easily. We will be interested in the light Higgs mass region, where we will have $\sin\theta \to 1$ for above mixing assignment. Finally, we point out that we can easily rewrite some of the coupling parameters as a function of the physical masses after SSB as follows [14, 33, 34]

$$\begin{aligned} \mu_{\phi \mathrm{h}} &= -\frac{2v_\phi}{v_h^2}\left(\sin^2\theta m^2_{h_1} + \cos^2\theta m^2_{h_2} + v_\phi\left(-2\lambda_\phi v_\phi + \mu_3\right)\right), \\ \lambda_{\phi \mathrm{h}} &= \frac{1}{v_h v_\phi}\left(\sin\theta\cos\theta\left(m^2_{h_2} - m^2_{h_1}\right) - v_h \mu_{\phi \mathrm{h}}\right), \\ \lambda_h &= \frac{1}{2v_h^2}\left(\sin^2\theta m^2_{h_2} + \cos^2\theta m^2_{h_1}\right). \end{aligned} \tag{3.10}$$

The freedom of choosing the other parameters will help us to get a correct Higgs mass even if we vary the following parameters to address correct relic density for DM in this model:

$$\{m_\chi, Y_{\chi\phi}, \sin\theta, \lambda_{\chi\phi}, \lambda_{\chi h}, m_{h_1}, v_\phi, \mu_\chi, \mu_{\chi\phi}, \lambda_\chi\} \tag{3.11}$$

After SSB the DM mass turns out to be : $m^2_\chi = \mu^2 + 1/2\lambda_{\chi\phi}v^2_\phi + \mu_{\chi\phi}v_\phi + 1/2\lambda_{\chi h}v^2_h$. Again, due to large number of parameters dictating DM mass, we will vary DM mass ($m_\chi, \mu_\chi, v_\phi, Y_{\chi phi}$) independently for available parameter space of the model.

3.2 Relic density outcome

The model at hand offers both SIMP-like and WIMP like solution as it has both self coupling and coupling to the SM. The SIMP like framework basically assumes a very tiny coupling with SM, which is realised here by $\lambda_{\chi h}$ and $\lambda_{\chi\phi}$ couplings. When we keep them very tiny, the $2_{DM} \to 2_{SM}$ annihilations will be subdued and one can explore the SIMP realization of the model. The Feynman diagrams that leads to $3_{DM} \to 2_{DM}$ number changing processes in

this framework are shown in Appendix B. There are four annihilation processes that dictate relic density of the DM, they are $\chi\chi\chi \to \chi\chi^*$, $\chi\chi^*\chi^* \to \chi\chi$ and their complex conjugate processes i.e. $\chi^*\chi^*\chi^* \to \chi^*\chi$ and $\chi^*\chi\chi \to \chi^*\chi^*$, respectively. The diagrams in each cases can be categorized into two classes, (i) mediated by self interaction of χ, (ii) mediated by the scalars h_1, h_2. We implemented this model using LanHEP [35]. To check the consistency with our numerical calculations, we have used CalcHEP [36], for drawing the Feynman diagrams we have used Tikz-Feynhand [37] and in order to calculate the matrix amplitudes, relic density using BEQ we have used Mathematica [38]. Vertex factors used in the calculation of each matrix amplitudes are also detailed in Appendix B. Here we note that the numerical solution to the SIMP like BEQ have been used to scan the parameter space to yield relic density, instead of the approximate analytical solution advocated before. As has been noted that there exists a little discrepancy in the values of relic density obtained in these two cases, particularly with low and high DM mass regions, although the main characteristics remain the same.

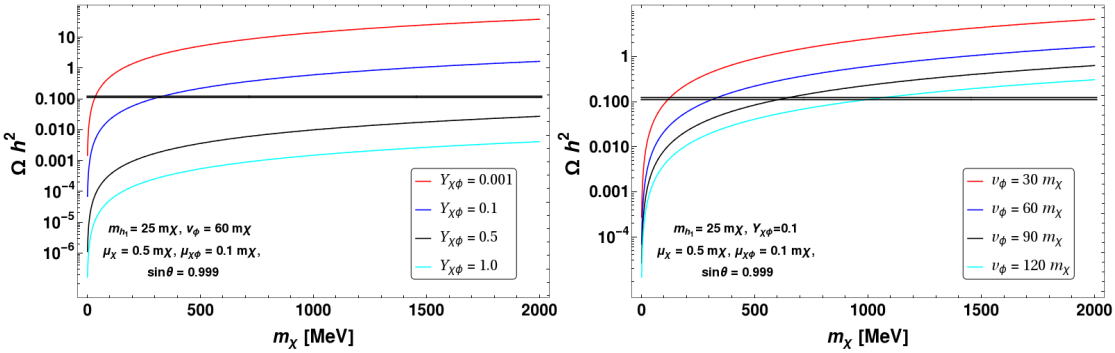

Figure 6: Variation of Relic density with DM mass for different values of $Y_{\chi\phi}$ [Left Panel] and v_ϕ [Right panel]. We kept the self coupling large ($\lambda_\chi = 1$) for both the plots. The correct relic density ($0.1177 \leq \Omega h^2 \leq 0.1221$) is also indicated here by the horizontal grey band.

It is straightforward to see that the matrix element squared for the complex conjugate processes are same:

$$|\mathcal{M}_{\chi\chi\chi\to\chi\chi^*}|^2 = |\mathcal{M}_{\chi^*\chi^*\chi^*\to\chi^*\chi}|^2, \;\; |\mathcal{M}_{\chi\chi^*\chi^*\to\chi\chi}|^2 = |\mathcal{M}_{\chi^*\chi\chi\to\chi^*\chi^*}|^2.$$

Therefore, the total $3 \to 2$ annihilation cross section in this model is given by:

$$\begin{aligned}\langle\sigma v^2\rangle_{3\to2} &= 2[\langle\sigma_{\chi\chi\chi\to\chi\chi^*}v^2\rangle + \langle\sigma_{\chi\chi^*\chi^*\to\chi\chi}v^2\rangle] \,, \\ &= \frac{2\sqrt{5}}{192\pi m_\chi^3}\left(|\mathcal{M}_{\chi\chi\chi\to\chi\chi^*}|^2 + |\mathcal{M}_{\chi\chi^*\chi^*\to\chi\chi}|^2\right),\end{aligned} \tag{3.12}$$

where the last line corresponds to s-wave computation of the annihilation cross section, also detailed in appendix B. For the SIMP realization, we need to keep the $2 \to 2$ annihilation to SM very small, therefore we choose $\lambda_{\chi\phi}$ and $\lambda_{\chi h}$ very tiny ~ 0.001. Since we are also interested in exploring the light Higgs mediation to expedite the annihilation processes, we have kept the value of mixing angle $\sin\theta = 0.999(\to 1)$. Keeping above parameters as quoted, we are now left with the following free parameters:

$$\{m_\chi, Y_{\chi\phi}, m_{h_1}, v_\phi, \mu_\chi, \mu_{\chi\phi}, \lambda_\chi\}. \tag{3.13}$$

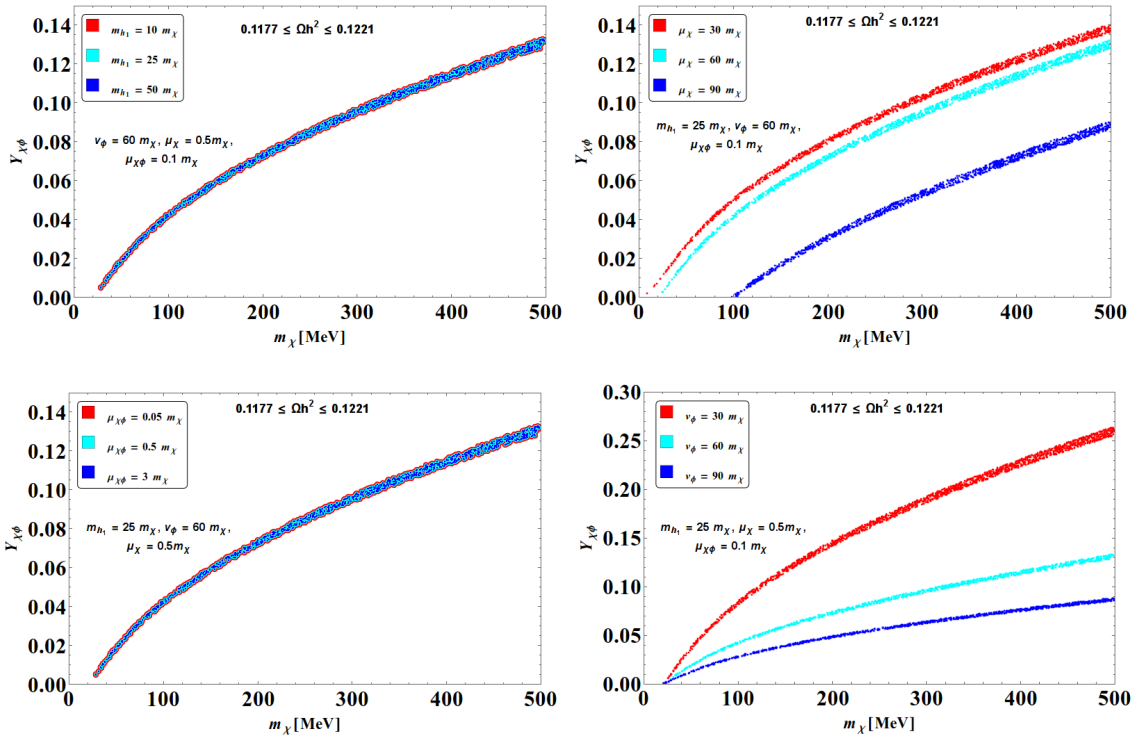

Figure 7: Relic density allowed ($0.1177 \leq \Omega h^2 \leq 0.1221$) parameter space in $m_\chi - Y_{\chi\phi}$ plane with variation of m_{h_1} (Top Left), μ_χ (Top Right), $\mu_{\chi\phi}$ (Bottom Left) and v_ϕ (Bottom Right). Other parameters kept fixed, and the range of variation are mentioned in the respective figure inset. We choose $\lambda_\chi = 1$ for illustration.

Now we will study the variation of relic density with DM mass, keeping most of the other parameters steady. In Fig. 6, we show such a variation with respect to different choices of $Y_{\chi\phi} \sim \{0.001 \to 1\}$ in the left panel and for different choices of $v_\phi \sim \{30m_\chi \to 120m_\chi\}$ in the right panel (the parameters kept constant are mentioned in the figure inset). We have kept $\lambda_\chi = 1$ for both the plots. The outcome from the left panel is understood easily, with larger $Y_{\chi\phi}$, the $3 \to 2$ annihilation gets larger and that diminishes the relic density significantly. Therefore, $Y_{\chi\phi}$ serves as one of the key parameters to find correct relic density in this model, and is used for the numerical scan performed later. Similarly, from the right panel, we see that v_ϕ turns out to be an important parameter to find the correct relic of this DM, as with larger v_ϕ, the annihilation cross-section increases and subsequently the relic density drops. The effects of $Y_{\chi\phi}$ and v_ϕ can also be validated from the expressions of annihilation cross-sections detailed in Appendix. As stated before, we use the numerical solution obtained from the BEQ.

Next in Fig. 7, we show the relic density allowed parameter space in $m_\chi - Y_{\chi\phi}$ plane by varying m_{h_1} (Top Left), μ_χ (Top Right), $\mu_{\chi\phi}$ (Bottom Left) and v_ϕ (Bottom Right) with other parameters fixed as mentioned in figure inset. We again choose $\lambda_\chi = 1$ for this plot. The available parameter space has a large DM mass range upto GeV with larger $Y_{\chi\phi}$ (going upto 0.4). We also see that variation in μ_χ and v_ϕ affect relic density quite significantly (top right and bottom right respectively) allowing a wide span of relic density allowed parameter space. This is easily seen from the vertex factors in Appendix B, that the three point vertex

is directly proportional to μ_χ and also on v_ϕ thanks to $\phi\chi^3$ term, which crucially controls the annihilation cross-section through self mediation. Again, note here that due to the freedom of having a large number of parameters contributing to $m_{h_{1,2}}$, we can fix Higgs mass (m_{h_2}) to 125 GeV and still vary m_{h_1} keeping $v_\phi = 60 m_\chi$ as in the top left panel.

To summarise this section, we see that a large parameter space is available from relic density constraint, particularly the DM mass can vary in a long range even upto GeV, while the relevant couplings $Y_{\chi\phi}, \lambda_\chi$ do not require to be very large. These are all in contrary to the naive SIMP realisation of DM ideally having one self coupling and one mass parameter dictating them to be in the strong interaction range. However, we need to consider other constraints like unitarity, vacuum stability and self scattering cross section, which will constrain the relic density allowed parameter space as we demonstrate below.

3.3 Additional Constraints on dark matter parameter space

In this section, we discuss three important constraints on the model parameter space namely vacuum stability, unitarity and self interaction cross-section. All the couplings are positive to cope up with the vacuum stability of the potential.

3.3.1 Self scattering cross section

DM self scatters through $2 \to 2$ scattering process like $\chi\chi \to \chi\chi$ and $\chi\chi^* \to \chi\chi^*$ and their complex conjugate processes. Again the Feynman graphs for such process in this model and their matrix element square calculations are detailed in Appendix. Therefore, the cross-section for such processes are obtained via:

$$\begin{aligned}\sigma_{self} &= 2[\sigma_{\chi\chi\to\chi\chi} + \sigma_{\chi\chi^*\to\chi\chi^*}] \\ &= \frac{2}{64\pi m_\chi^2}\left(|\mathcal{M}_{\chi\chi\to\chi\chi}|^2 + |\mathcal{M}_{\chi\chi^*\to\chi\chi^*}|^2\right).\end{aligned}$$

Again, we have used the fact that the matrix element for $\chi\chi \to \chi\chi$ and $\chi^*\chi^* \to \chi^*\chi^*$ are same. There are two important bounds on the self scattering cross-section for DM coming from Bullet cluster and Abell cluster data as follows.

- Bullet cluster bound [15]:

$$\sigma_{self}/m_\chi \lesssim 1 \text{ cm}^2/g \quad (= 4555.8 \text{ GeV}^{-3}) \tag{3.14}$$

- Abell cluster bound [16]:

$$1 \lesssim \sigma_{self}/m_\chi \lesssim 3 \text{ cm}^2/g \tag{3.15}$$

As one can clearly see that the bounds above do not agree to each other. We will use one or the other to see the constraints on the model parameter space.

3.3.2 Unitarity Bound

Unitarity of S matrix constrains the matrix element of the $2 \to 2$ scattering process via [3]

$$|\mathcal{M}_{\chi\chi\to\chi\chi}| \leq 8\pi, \ |\mathcal{M}_{\chi\chi^*\to\chi\chi^*}| \leq 8\pi \tag{3.16}$$

[3] This can be derived from optical theorem using partial wave analysis [39].

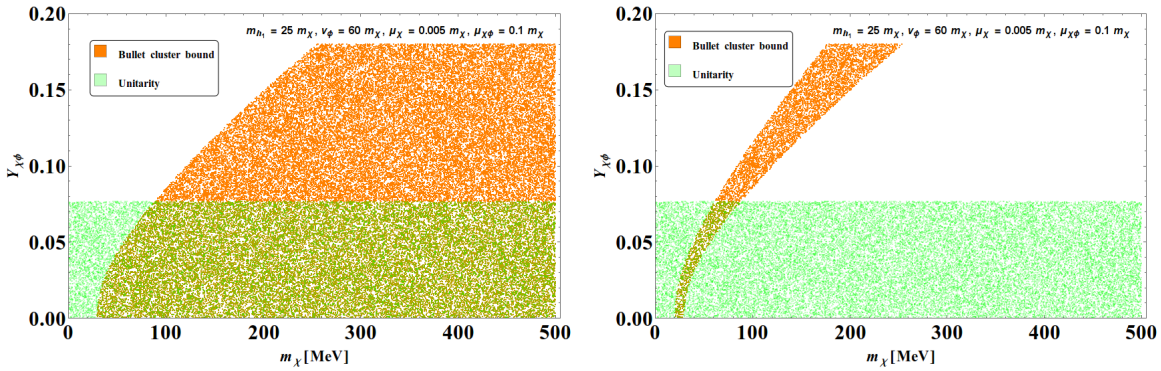

Figure 8: Unitarity Bound (Green) and Self scattering cross-section limit (Orange) in $m_\chi - Y_{\chi\phi}$ plane of our model. We have kept other parameters fixed as mentioned in the figure inset. Bullet Cluster bound (Eq. 3.14) is shown in the left panel and Abell Cluster bound (Eq. 3.15) is shown in the right panel. We have kept $\lambda_\chi = 1$ for this plot.

It turns out to be one of the most stringent bounds on the model parameter space as we demonstrate below. In addition, we also obey the perturbative limit on each of the couplings assumed in the model $|\lambda_i| < 4\pi$.

In Fig. 8, we have plotted the available parameter space in $m_\chi - Y_{\chi\phi}$ plane of our model coming from self scattering cross-section limits from Bullet cluster data (Eq. 3.14) in the left panel and Abell cluster data (Eq. 3.15) in the right panel by green shaded region together with unitarity bound by orange shaded region. The plot is obtained by keeping $\lambda_\chi = 1$, while other choices of parameters are mentioned in the figure inset. Unitarity bound strongly constrains $Y_\chi\phi \lesssim 0.07$.

3.4 Summary of available parameter space from all constraints

In this section we will show the available parameter space which satisfy all the bounds together from unitarity, self scattering and relic density for different choices of model parameters.

In Fig. 9, we put together relic density, unitarity bound and self scattering constraint arising from Bullet cluster in the left panel. The right panel figure shows the available parameter space after all these constraints in $Y_{\chi\phi} - m_\chi$ plane. There are two important conclusions that we obtain from here: (i) the mass range of the DM is limited to ~ 200 MeV, while the coupling is restricted to a very small, $Y_{\chi\phi} \sim \{0.02 \to 0.08\}$. This is obtained with $\lambda_\chi = 1$ that we choose for this particular scan. We will show later that changing λ_χ to ~ 0.1 will not change the order of $Y_{\chi\phi}$ significantly. A similar scan is presented in Fig. 10, but with self scattering cross-section dictated by Abell cluster constraint. The available parameter space is further restricted for this case to remain within ~ 40 GeV (right panel of Fig. 10). The other relevant parameters have been kept constant and mentioned in figure inset.

In Fig. 11, we show how the allowed parameter space changes due to different choices of v_ϕ. Smaller v_ϕ requires larger $Y_{\chi\phi}$ to keep the annihilation cross-section to right ball park. Similarly in Fig. 12, we show how the available parameter space changes due to different choices of μ_χ which also serves as an important parameter of the model. The behaviour is similar to v_ϕ. With larger μ_χ, the coupling $Y_{\chi\phi}$ requires to be smaller to adjust right annihilation cross-section. We would also mention that in the right panel of Fig. 12,

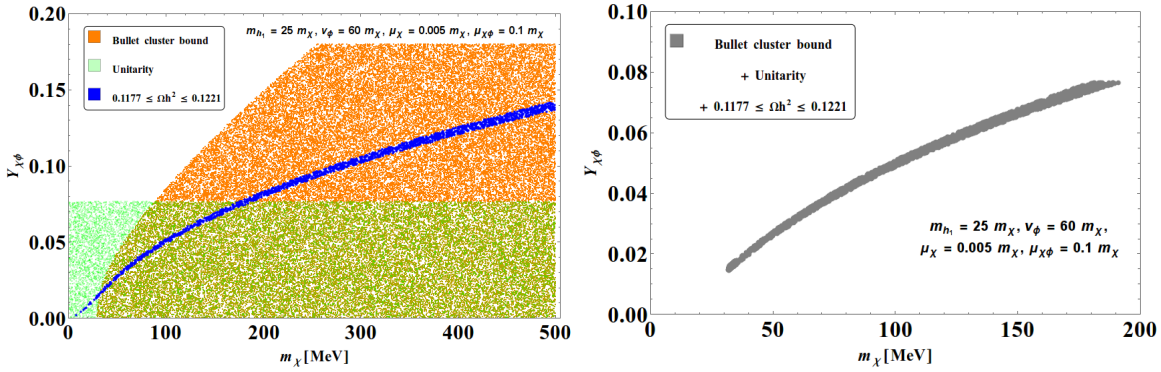

Figure 9: [Left Panel] Self scattering bound for Bullet cluster (Orange), Unitarity (Green) and Relic density (Blue) allowed regions are plotted in $m_\chi - Y_{\chi\phi}$ plane where the other parameters are mentioned inside the figure. [Right Panel] Combined parameter space allowed from all the bounds.

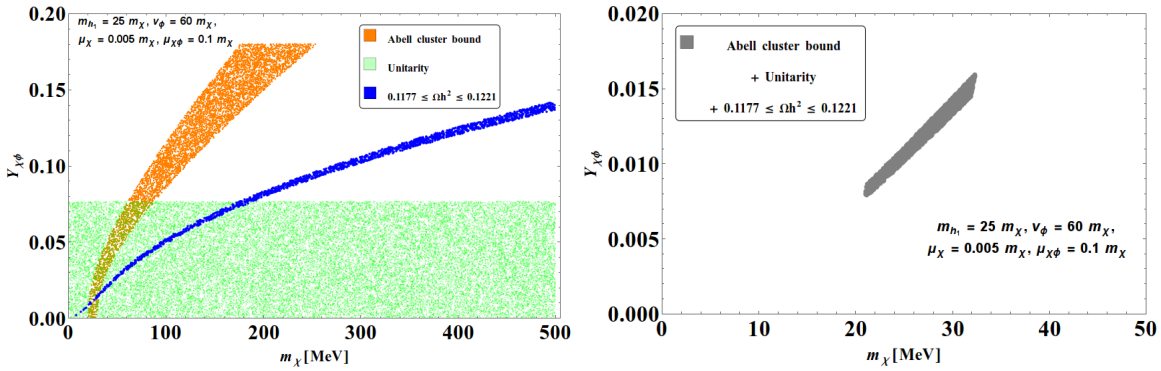

Figure 10: [Left Panel] Self scattering bound for Abell cluster (Orange), Unitarity (Green) and Relic density (Blue) allowed regions are plotted in $m_\chi - Y_{\chi\phi}$ plane where the other parameters are mentioned inside the figure. [Right Panel] Combined parameter space for all Bounds.

the bound from Abell cluster data do not yield a viable parameter space for the choice of $\mu_\chi = 3m_\chi$, while keeping $Y_{\chi\phi}$ positive.

Next we choose to illustrate the importance of λ_χ parameter of the model. In Fig. 13, we show the available parameter space of the model in $m_\chi - Y_{\chi\phi}$ plane for different choices of λ_χ from relic density, unitarity and self scattering cross-section. Interestingly, we see that a common parameter space is available even after choosing $\lambda_\chi = 0.1$. Finally, we show the importance of having the additional scalar (ϕ) in our model to yield a larger parameter space from all the constraints. This is shown in Fig. 14 in $m_\chi - \lambda_\chi$ plane, where in the left plot we scan our model and in the right panel the case in absence of ϕ is demonstrated. We clearly identify that while our model (left) can have a large range of DM masses allowed by the freedom of choosing large λ_χ, the model in absence of ϕ, leaves in a constrained region with DM mass ranging between $30 - 80$ MeV.

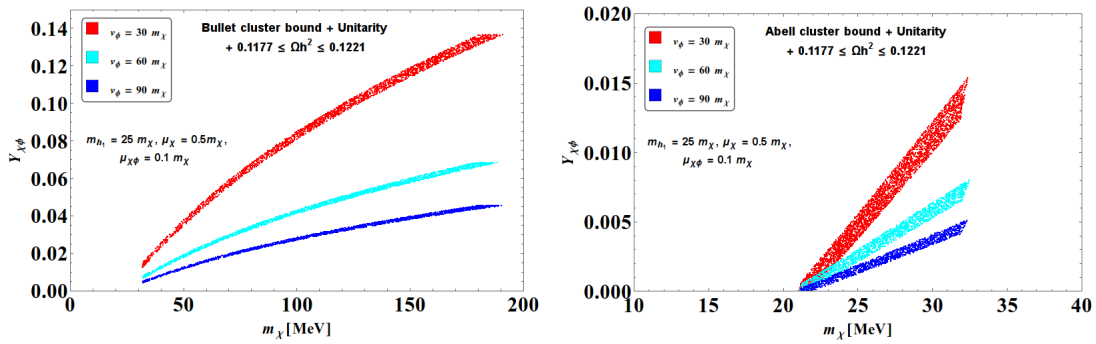

Figure 11: Allowed parameter space in $m_\chi - Y_{\chi\phi}$ plane for different choices of v_ϕ from relic density, unitarity and self scattering cross-section coming from [Left Panel] Bullet Cluster, [Right Panel] Abell Cluster constraints.

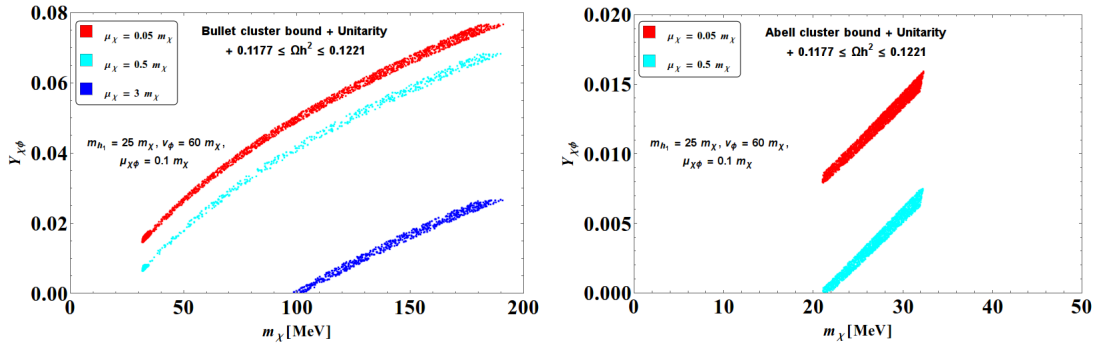

Figure 12: Allowed parameter space in $m_\chi - Y_{\chi\phi}$ plane for different choices of μ_χ from relic density, unitarity and self scattering cross-section coming from [Left Panel] Bullet Cluster, [Right Panel] Abell Cluster constraints.

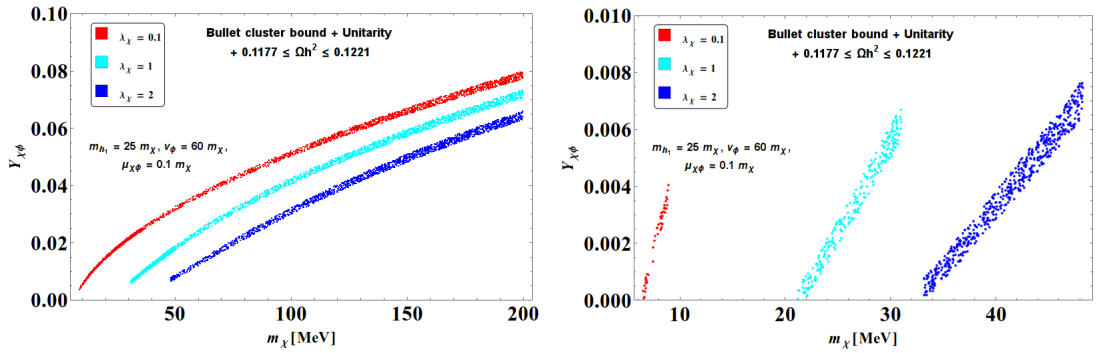

Figure 13: Allowed parameter space in $m_\chi - Y_{\chi\phi}$ plane for different choices of λ_χ from relic density, unitarity and self scattering cross-section.

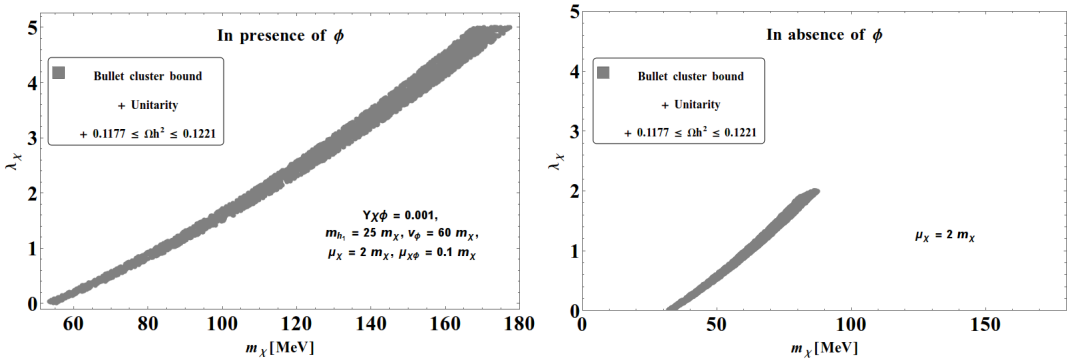

Figure 14: Allowed parameter space in $m_\chi - \lambda_\chi$ plane from relic density, unitarity and self scattering cross-section [Left Panel] our model, [Right Panel] model in absence of ϕ.

3.5 What keeps the DM in equilibrium in SIMP realisation ?

As we have argued before, that SIMP realisation of this model crucially depends on the fact that $2 \to 2$ annihilation to SM is negligible and that has been ensured by vanishingly small $\lambda_\chi h$ and $\lambda_\chi \phi$ in our model so that thermal freeze-out is governed by $3 \to 2$ annihilation in dark sector. Then the question is what keeps the DM in equilibrium in the early universe or what ensures the inequality described in Eq. 2.11. Here we demonstrate the estimate that $2 \to 2$ scattering is still way larger than the $2 \to 2$ annihilation in the model. We note first that the ratio of the rate of scattering versus annihilation in $2 \to 2$ reads as:

$$\frac{\Gamma_{kin}}{\Gamma_{ann}} = \frac{n_{SM}\langle\sigma v\rangle_{\chi f \to \chi f}}{n_{DM}\langle\sigma v\rangle_{\chi\chi^* \to f\bar{f}}} \tag{3.17}$$

In above equation, the distinction comes from annihilation and scattering cross section together with the number density of SM and DM given by

$$\begin{aligned} n_{SM} &= \frac{3}{2\pi^2}\zeta(3)T^3 \ , \\ n_{DM}(x) &= Y(x)\frac{2\pi^2}{45}g_{*s}T^3, \qquad (g_{*s} = 10.75) \end{aligned} \tag{3.18}$$

where $Y(x)$ is the co moving number density and can be found out by solving BEQ for $2 \to 2$ annihilation to SM, i.e.

$$\frac{dY}{dx} = -(0.264 * g_{*s}^{1/2}\ M_{pl}\ m_\chi/x^2)\langle\sigma v\rangle_{\chi\chi^* \to \bar{f}f}(Y^2 - Y_{eq}^2) \ . \tag{3.19}$$

Now, $\langle\sigma v\rangle_{\chi\chi^* \to f\bar{f}}$ in s-wave approximation is given by:

$$\langle\sigma v\rangle_{\chi\chi^* \to f\bar{f}} = \frac{1}{16\pi m_\chi^2}|\mathcal{M}_{\chi\chi^* \to f\bar{f}}|^2. \tag{3.20}$$

We find that matrix element squared for annihilation cross-section turns out:

$$|\mathcal{M}_{\chi\chi^* \to f\bar{f}}|^2 = 2 \times 2(s - 4m_f^2)\left[\frac{\lambda_{a1}\lambda_{f_1}}{(s - m_{h_1}^2)^2} + \frac{\lambda_{b1}\lambda_{f_2}}{(s - m_{h_2}^2)^2}\right]^2 \ . \tag{3.21}$$

Now the scattering cross-section in s-wave approximation reads as:

$$\langle \sigma v \rangle_{\chi f \to \chi f} = \frac{1}{8\pi m_\chi^2} |\mathcal{M}_{\chi f \to \chi f}|^2 \ . \tag{3.22}$$

Using the vertices available in the model, the matrix element squared for the scattering process turns out to be:

$$|\mathcal{M}_{\chi f \to \chi f}|^2 = 2 \times (-2)(t - 4m_f^2) \left[\frac{\lambda_{a1}\lambda_{f_1}}{(t - m_{h_1}^2)^2} + \frac{\lambda_{b1}\lambda_{f_2}}{(t - m_{h_2}^2)^2} \right]^2 \ . \tag{3.23}$$

Here we use, $m_f \to$ mass of SM fermion.

If we choose the DM mass of 15 MeV, and $\lambda_{\chi\phi} = \lambda_{\chi h} = 0.001$, it is easy to check that both annihilation cross-section Eq. (3.22) and scattering cross-section Eq. (3.20) are of the same order $\sim \mathcal{O}(10^{-15})$ i.e. negligible. Therefore, we can rewrite the ratio between the scattering rate to annihilation rate Eq. (3.17) as the ratio of SM versus DM number density:

$$\frac{\Gamma_{kin}}{\Gamma_{ann}} = \frac{n_{SM}}{n_{DM}} = \frac{\frac{3}{2\pi^2}\zeta(3)T^3}{Y(x)\frac{2\pi^2}{45}g_{*s}T^3} \tag{3.24}$$

Using $x = 15$, we find that

$$\frac{\Gamma_{kin}}{\Gamma_{ann}} = \frac{135\zeta(3)T^3}{Y(x)4\pi^4 g_{*s}T^3} \sim O(10^6). \tag{3.25}$$

So that it satisfy the SIMP condition and keeps the dark sector cool.

Here, we also point out that of $3 \to 2$ annihilations to SM in this model is also non negligible. The BEQ when two of these processes ($3 \to 2$ within dark sector and $3 \to 2$ in SM) contribute together look like following:

$$\begin{aligned} \frac{dY}{dx} = -((0.115\ g_{*s}^{3/2}\ M_{pl}\ m_\chi^4)/x^5) \Big[& (\langle \sigma v \rangle_{\chi\chi\chi \to \chi\chi} + \langle \sigma v \rangle_{\chi\chi^*\chi^* \to \chi\chi})(Y^3 - Y^2 Y_{eq}) \\ & + \langle \sigma v \rangle_{\chi\chi\chi \to f\bar{f}}(Y^3 - Y_{eq}^3) \\ & + \langle \sigma v \rangle_{\chi\chi f \to \chi^* f}(Y^2 Y_{eq} - Y Y_{eq}^2) \Big] \end{aligned} \tag{3.26}$$

In Fig. 15, we demonstrate the freeze-out in such a case. In the top panel, we show the case when DM freeze-out through $3_{\rm DM} \to 2_{\rm SM}$ only. The solution shows that $3_{\rm DM} \to 2_{\rm SM}$ interaction is good enough to keep the DM follow equilibrium distribution at low x and yields a typical but early freeze-out. On the bottom left panel, when we include additionally the annihilation for DM through $3_{\rm DM} \to 2_{\rm DM}$ in the dark sector, due to enhanced self coupling (as chosen for the SIMP like case), the number changing process in the dark sector dominates over $3_{\rm DM} \to 2_{\rm SM}$ and yields a free-out that corresponds to correct relic. This is validated by taking $3_{\rm DM} \to 2_{\rm DM}$ annihilation in the dark sector *only* (as we have done for the analysis) in the bottom right panel to show that the freeze-out mimics the case of taking both contributions together (as in bottom left Fig) and justifies our analysis.

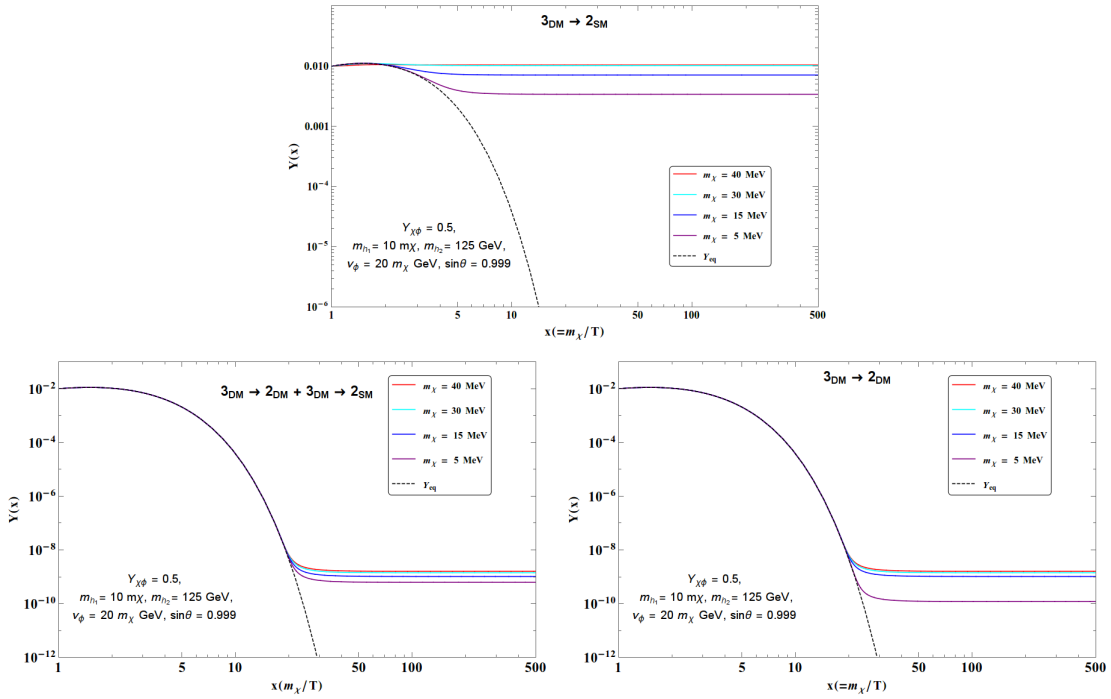

Figure 15: Freeze-out of DM χ from thermal equilibrium in $Y(x) - x$ plane in presence of $3_{\rm DM} \to 2_{\rm SM}$ i.e. annihilation to SM only [top], $3_{\rm DM} \to 2_{\rm DM,SM}$ i.e. annihilation to DM and SM [bottom left] and $3_{\rm DM} \to 2_{\rm DM}$ i.e. annihilation to DM only [bottom right].

4 WIMP realisation of the model

Finally for comparison, we demonstrate the WIMP realisation of the same model that we have studied in this paper. The BEQ in WIMP scenario is given by:

$$\frac{dY}{dx} = -\left[\frac{(0.264*g_{*s}^{1/2}\times M_{pl}\times m_\chi)}{x^2}\langle\sigma v\rangle_{2_{DM}\to 2_{SM}}(Y^2 - Y_{eq}^2) + \frac{(0.115*g_{*s}^{3/2}\times M_{pl}\times m_\chi^4)}{x^5}\langle\sigma v^2\rangle_{3_{DM}\to 2_{DM}}(Y^3 - Y^2 Y_{eq})\right]. \tag{4.1}$$

In the above Eqn. 4.1, we have considered the DM annihilation to SM through $2_{DM} \to 2_{SM}$ and also the one used for SIMP condition, namely $3_{DM} \to 2_{DM}$ process. The corresponding annihilation channels and the cross-sections are elaborated in Appendix. DM freeze-out is shown in Fig. 16 for three cases: (i) considering only $2_{DM} \to 2_{SM}$ (blue line), (ii) only $3_{DM} \to 2_{SM}$ (cyan line), (iii) the actual situation $2_{DM} \to 2_{SM}$ and $3_{DM} \to 2_{SM}$ together (red dashed) following Eqn. 4.1. We clearly see here that $3_{DM} \to 2_{SM}$ annihilation has a very small contribution as the lone process of such kind will yield an early freeze-out, whereas when considered together with $2_{DM} \to 2_{SM}$, can not be distinguished from the case (iii) where $2_{DM} \to 2_{SM}$ and $3_{DM} \to 2_{SM}$ are addressed together. Therefore, it is quite justified to neglect the second term in BEQ 4.1 for WIMP solution.

As has already been mentioned that SIMP realisation of this model was possible by choosing the coupling to SM very feeble, namely keeping $\lambda_{\chi\phi} = \lambda_{\chi h} \sim 0.001$, altering which the $2 \to 2$ annihilation to SM dominates over the $3 \to 2$ in dark sector and governs the freeze-out to reveal WIMP paradigm of the model. We show next the variation in relic

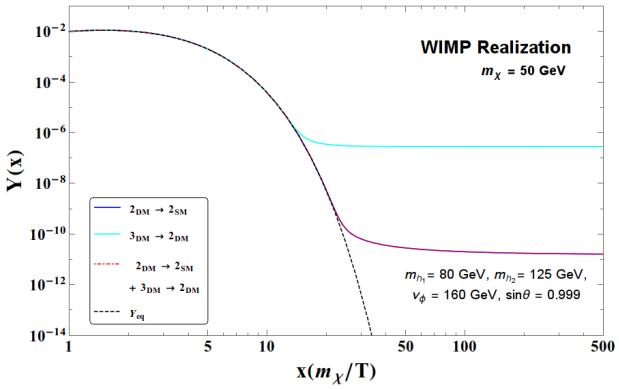

Figure 16: DM freeze out in WIMP scenario following the BEQ given in (4.1) with three choices of DM annihilation: (i) $2_{DM} \to 2_{SM}$ (blue line), (ii) $3_{DM} \to 2_{SM}$ (cyan line), (iii) $2_{DM} \to 2_{SM}$ and $3_{DM} \to 2_{SM}$ together (red dashed). The cases of (i) and (iii) superimpose on each other. We choose DM mass of $\sim$ 50 GeV, and DM-SM couplings of the order of $\lambda_{\chi\phi} = \lambda_{\chi h} \sim 0.1$.

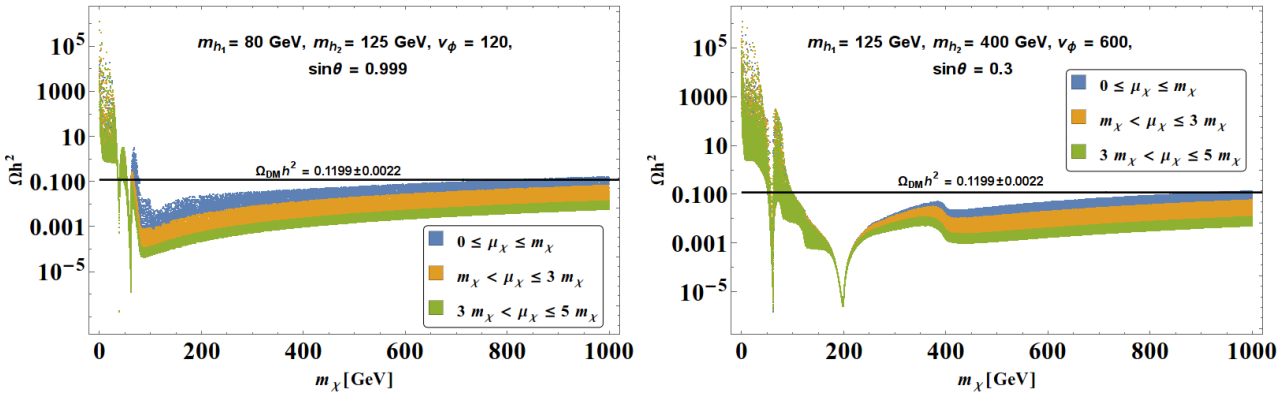

Figure 17: Relic density in WIMP condition for DM χ as a function of DM mass, with the variation in μ_χ. All the parameters kept constant are mentioned in figure inset. Notably we have chosen larger $\lambda_{\chi\phi} = \lambda_{\chi h} \sim 0.1$.

density with DM mass in Fig. 17 for WIMP realisation of the model. We choose to illustrate two different values of the additional scalar boson mass: a light scalar mass of 80 GeV for the left plot and a heavy scalar of 400 GeV in the right plot. To compute relic density and direct search cross section for the model we have used micrOmegas [40]. We see that two resonance drops at $m_{h_{1,2}}/2$ are clearly observed for s-channel mediation of $h_{1,2}$ in $2 \to 2$ annihilation process. We also point out the variation in μ_χ for illustration, the larger the μ_χ, the larger is the annihilation cross-section and therefore smaller is the relic density. There exist a semi-annihilation effect $\chi\chi \to h\chi$ for the WIMP DM here that helps disentangling the relic density to direct search; but, to drop below the direct search constraints require a large μ_χ, that lies in tension with vacuum stability.

We next analyse the constraint coming from direct search to the relic density allowed parameter space of the WIMP scenario of the model. The Feynman graph for direct search interaction is shown in Fig. 18 through t-channel $h_{1,2}$ mediation. The scan for relic density

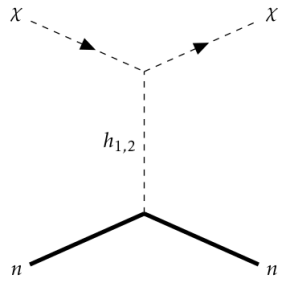

Figure 18: Feynman graph for Direct Search interaction of DM (χ) with nucleon (n) through $h_{1,2}$ mediation in WIMP scenario.

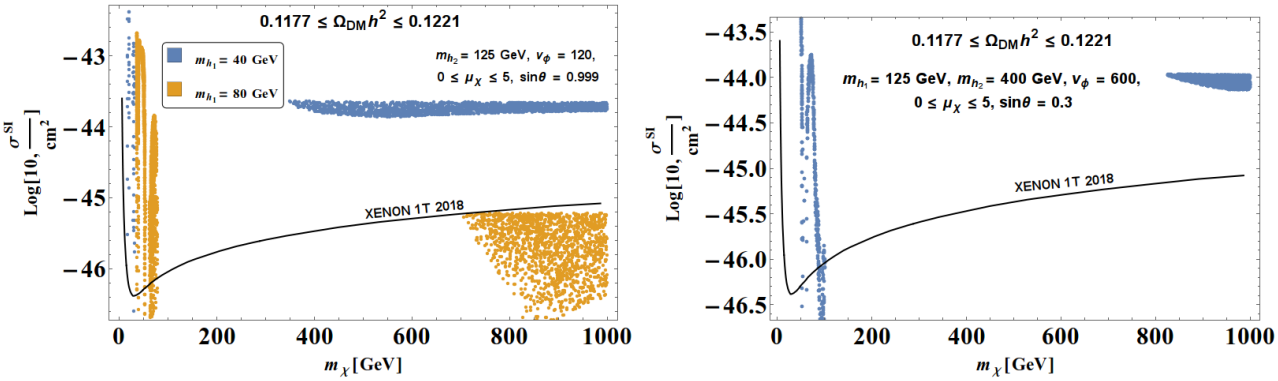

Figure 19: Direct detection bound (XENON1T) on relic density allowed parameter space of the WIMP DM χ. We scan low Higgs mass ($m_{h_1} = 40$ GeV [blue] and $= 80$ GeV [golden yellow]) on the Left panel, and heavy Higgs mass ($m_{h_2} = 400$ GeV) on the right panel. Other parameters are kept steady as mentioned in figure inset.

allowed parameter space of the model in spin independent direct search cross section versus DM mass plane is shown in Fig. 19. We have chosen two different possible phenomenological situations for illustration: light additional scalar ($m_{h_1} = 40$ GeV in blue and $m_{h_1} = 80$ GeV in golden yellow) on the left panel and heavy scalar ($m_{h_2} = 400$ GeV) on the right panel. The main outcome of this analysis is to see that immaterial to the additional scalar mass resonance regions are allowed by direct search. Interestingly, when the additional scalar mass is not too far from the SM Higgs, as is the case for $m_{h_1} = 80$ GeV as shown by golden yellow points in the left panel, there is a large region of heavy DM mass ($\sim 800 \to 1000$ GeV), which becomes allowed by direct search constraint. This can be explained by realizing that since the spin independent direct search cross-section follows [34]:

$$\sigma_{DD}^{SI} = \frac{1}{4\pi}\left(\frac{f_n \mu_n}{m_\chi}\right)^2 \left(\frac{m_n}{v_h}\right)^2 \left[\frac{\lambda_{a1}\cos\theta}{m_{h_1}^2} + \frac{\lambda_{b1}\sin\theta}{m_{h_2^2}}\right]^2 , \tag{4.2}$$

where λ_{a1} and λ_{b1} are DM-Higgs coupling, f_n is the form factor, $\mu_n = m_n m_\chi/(m_n + m_\chi)$ is the reduced mass. The cross-section yields a destructive interference due to opposite sign of λ_{a1} and λ_{b1} (look at the Table 2 of vertices in Appendix A) when the two scalar masses are close.

5 Summary and Conclusion

We have presented a model where both SIMP and WIMP realization of a scalar DM is possible. This is achieved by assuming a complex scalar field χ which transforms under un unbroken Z_3. When the portal coupling is small it provides a SIMP solution and when the portal coupling is large, it provides a WIMP like solution. In principle, this bit of model construct is good enough to realise the correct relic density in a SIMP condition and perhaps serves as the simplest SIMP DM, where the number changing process within the dark sector is solely governed by DM self coupling. However, we add to that another scalar field ϕ that is even under Z_3, acquires a vev, mixes with SM Higgs and serves as a light scalar mediator to aid DM self scattering to yield a large parameter space available to the model. We also see that due to the presence of this additional field, the coupling to achieve a successful SIMP DM do not require to be that large of strong interaction limit. Relic density allows the mass range of the DM to be within a large range even upto $\sim$ GeV, which gets further restricted from the self scattering constraints and unitarity bound. For Bullet cluster the bound turns out to be within ~ 200 MeV range, while for Abell cluster data, the bound is more restrictive and remains within ~ 50 MeV.

We also analyse the WIMP limit of the DM for the sake of comparison. Interestingly the direct search allowed parameter space for such a framework predict that the additional Higgs mass should be close to the SM Higgs due to a destructive interference in the direct search cross-section. On the other hand SIMP realisation is aided when the additional scalar is light of the order of sub-GeV. it is important to remind that such a scalar is quite likely to evade the collider search bound due to its singlet nature.

Thermal freeze out of the DM in SIMP condition for $3 \to 2$ number changing process is performed in details and we advocate an approximate analytical solution for relic density which yields agreement to the numerical solution for a certain range of DM mass. We also calculate all the cross-sections for freeze out and self scattering in details, so that the draft serves as a useful reference for performing phenomenological analysis in any SIMP framework.

Acknowledgement

SV acknowledges to the BTP project at the department of Physics in IIT Guwahati, where the project was initiated. SB and SV also acknowledges DST-INSPIRE Faculty grant IFA-13 PH-57. PG would like to thank MHRD, Government of India for research fellowship.

Appendix

A Vertices and Couplings of the model

Here we list all the vertices that appear in the cross-sections for annihilation and scattering processes in this model. We also introduce a notation that will be used further in computing the amplitudes.

Vertices	Vertex factor	Notation
$\chi^*\chi\chi^*\chi$	$-(2!2!)\,\lambda_\chi = -4\lambda_\chi$	$-\lambda_4$
$\chi\chi\chi$	$-\frac{(\mu_\chi+Y_{\chi\phi}v_\phi)}{6}3! = -(\mu_\chi + Y_{\chi\phi}v_\phi)$	$-\lambda_3$
$\chi^*\chi h_1$	$-(\lambda_{\chi h}v_h\cos\theta - (\lambda_{\chi\phi}v_\phi + \mu_{\chi\phi})\sin\theta)$	$-\lambda_{a1}$
$\chi^*\chi h_2$	$-(\lambda_{\chi h}v_h\sin\theta + (\lambda_{\chi\phi}v_\phi + \mu_{\chi\phi})\cos\theta)$	$-\lambda_{b1}$
$\chi\chi\chi h_1$	$-(-\sin\theta Y_{\chi\phi})$	$-\lambda_{a2}$
$\chi\chi\chi h_2$	$-(-\cos\theta Y_{\chi\phi})$	$-\lambda_{b2}$
$f\bar{f}h_1$	$-\frac{m_f}{v}\cos\theta$	$-\lambda_{f1}$
$f\bar{f}h_2$	$-\frac{m_f}{v}\sin\theta$	$-\lambda_{f2}$

Table 2: Couplings (in terms of the model parameters, see Eq. 3.3) that appear in the model and is required for computing all the processes considered in this analysis. Short hand notations are introduced.

B Annihilation cross-section for $3_{\rm DM} \to 2_{\rm DM}$ process

We first note that the dominant contribution in absence of $2 \to 2$ annihilations to SM are $3_{\rm DM} \to 2_{\rm DM}$ that yields the required freeze out. Apart from χ mediation, the two other mediators for such diagrams are the two Higgses, which are mentioned by the following notation in the matrix element.

$$a \Rightarrow h_1 \text{ mediation}$$
$$b \Rightarrow h_2 \text{ mediation}$$

There are two major processes in the model which contribute to such a case: $\chi\chi\chi \to \chi\chi^*$ and $\chi\chi^*\chi^* \to \chi\chi$ and their conjugates. We will analyse them systematically below.

$\chi\chi\chi \to \chi\chi^*$

Feynman Diagrams

Only $h_{1,2}$ Mediated

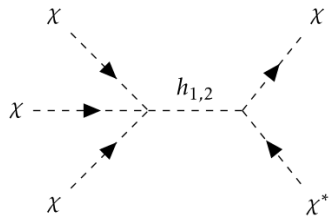

1a, 1b

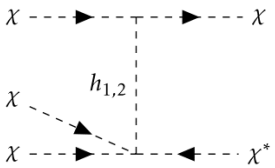

2a, 2b

$h_{1,2}$ and χ Mediated

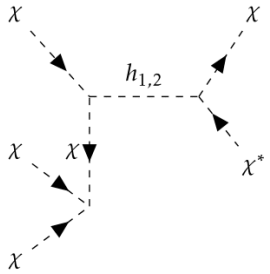

3a, 3b

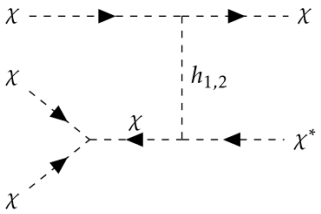

4a, 4b

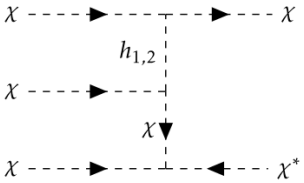

5a, 5b

Only χ Mediated

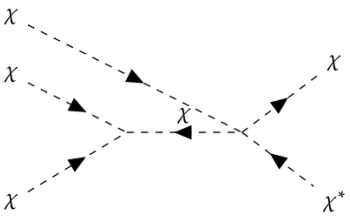

6

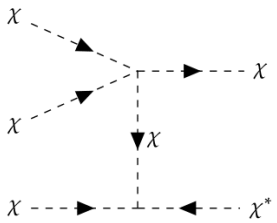

7

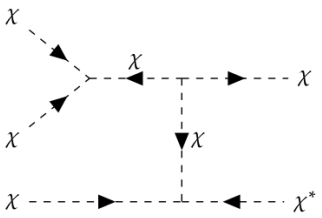

8

Matrix Amplitude

Only $h_{1,2}$ mediated

- $\mathcal{M}_{1a} = \frac{(-\lambda_{a1})(-\lambda_{a2})}{s-m_{h_1}^2}$
- $\mathcal{M}_{2a} = \frac{(-\lambda_{a1})(-\lambda_{a2})}{t-m_{h_1}^2}$
- $\mathcal{M}_{1b} = \frac{(-\lambda_{b1})(-\lambda_{b2})}{s-m_{h_2}^2}$
- $\mathcal{M}_{2b} = \frac{(-\lambda_{b1})(-\lambda_{b2})}{t-m_{h_2}^2}$

$h_{1,2}$ and χ mediated

- $\mathcal{M}_{3a} = \frac{(-\lambda_{a1})^2(-\lambda_3)}{(s-m_{h_1}^2)(t-m_\chi^2)}$
- $\mathcal{M}_{4a} = \frac{(-\lambda_{a1})^2(-\lambda_3)}{(t-m_{h_1}^2)(s-m_\chi^2)}$
- $\mathcal{M}_{5a} = \frac{(-\lambda_{a1})^2(-\lambda_3)}{(t-m_{h_1}^2)(t-m_\chi^2)}$
- $\mathcal{M}_{3b} = \frac{(-\lambda_{b1})^2(-\lambda_3)}{(s-m_{h_2}^2)(t-m_\chi^2)}$
- $\mathcal{M}_{4b} = \frac{(-\lambda_{b1})^2(-\lambda_3)}{(t-m_{h_2}^2)(s-m_\chi^2)}$
- $\mathcal{M}_{5b} = \frac{(-\lambda_{b1})^2(-\lambda_3)}{(t-m_{h_2}^2)(t-m_\chi^2)}$

Only χ mediated

- $\mathcal{M}_6 = \frac{(-\lambda_3)(-\lambda_4)}{s-m_\chi^2}$
- $\mathcal{M}_7 = \frac{(-\lambda_3)(-\lambda_4)}{t-m_\chi^2}$
- $\mathcal{M}_8 = \frac{(-\lambda_3)^3}{(s-m_\chi^2)(t-m_\chi^2)}$

$$\mathcal{M}_{net} = (\mathcal{M}_{1a} + \mathcal{M}_{2a} + \mathcal{M}_{3a} + \mathcal{M}_{4a} + \mathcal{M}_{5a}) + (\mathcal{M}_{1b} + \mathcal{M}_{2b} + \mathcal{M}_{3b} + \mathcal{M}_{4b} + \mathcal{M}_{5b}) + \mathcal{M}_6 + \mathcal{M}_7 + \mathcal{M}_8$$

Squared matrix amplitude is given as,

$$\Rightarrow |\mathcal{M}_{\chi\chi\chi\to\chi\chi^*}|^2 = |\mathcal{M}_{Net}|^2$$

The complex conjugate of $\chi\chi\chi \to \chi\chi^*$ *i.e.* $\chi^*\chi^*\chi^* \to \chi^*\chi$ also contributes to the total matrix amplitude and has same expression as $\chi\chi\chi \to \chi\chi^*$,

$$|\mathcal{M}_{\chi\chi\chi\to\chi\chi^*}|^2 = |\mathcal{M}_{\chi^*\chi^*\chi^*\to\chi^*\chi}|^2$$

Therefore the cross-section reads:

$$\begin{aligned}\langle\sigma_{\chi\chi\chi\to\chi\chi^*}v^2\rangle &= \frac{\sqrt{5}}{192\pi m_\chi^3}\left[|\mathcal{M}_{\chi\chi\chi\to\chi\chi^*}|^2 + |\mathcal{M}_{\chi^*\chi^*\chi^*\to\chi^*\chi}|^2\right] \\ &= \frac{\sqrt{5}}{192\pi m_\chi^3}\left[2 * |\mathcal{M}_{\chi\chi\chi\to\chi\chi^*}|^2\right] \end{aligned} \tag{B.1}$$

We will derive the last expression in a moment.

$\chi\chi^*\chi^* \to \chi\chi$

Feynman Diagrams

Only $h_{1,2}$ Mediated

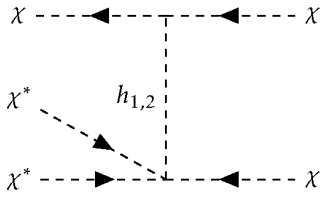

1a, 1b

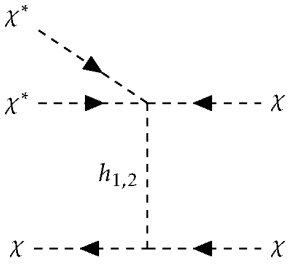

2a, 2b

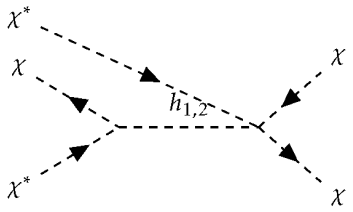

3a, 3b

$h_{1,2}$ and χ mediated

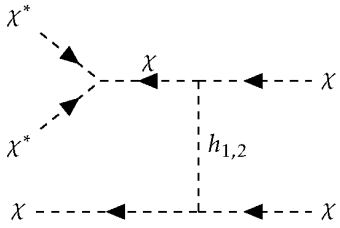

4a, 4b

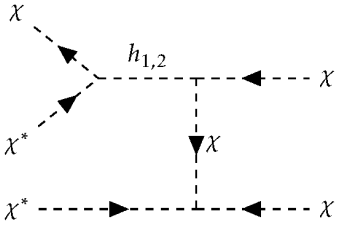

5a, 5b

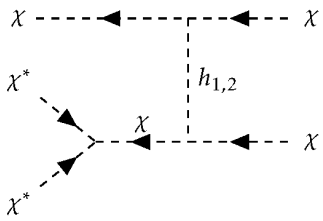

6a, 6b

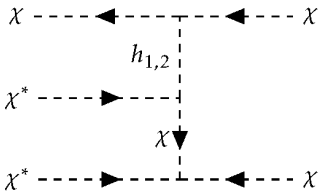

(a) 7a, 7b

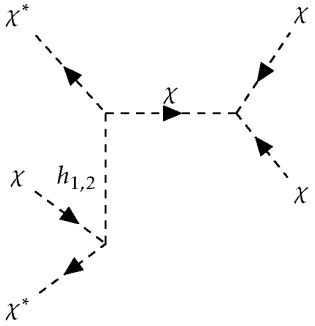

(b) 8a, 8b

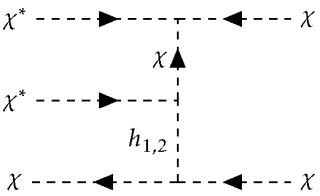

(c) 9a, 9b

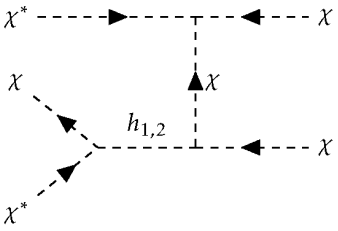

(a) 10a, 10b

Only χ mediated

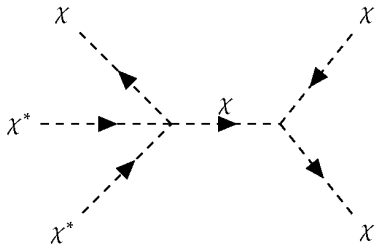

(a) 11

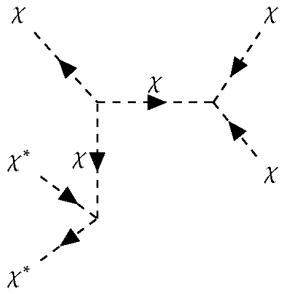

(b) 12

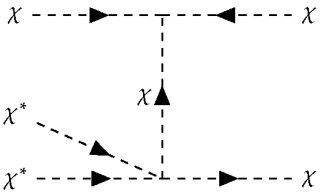

(c) 13

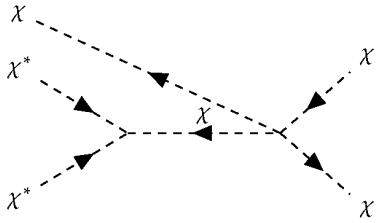

(a) 14

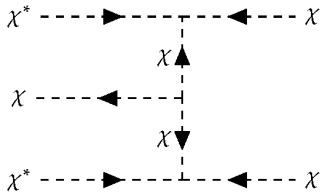

(b) 15

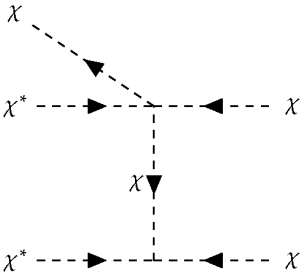

(c) 16

Note here that we have omitted $u-$ channel graphs, which will also contribute to the cross-section.

Matrix Amplitude

Only χ mediated

- $\mathcal{M}_{11} = \frac{(-\lambda_3)(-\lambda_4)}{s-m_\chi^2}$
- $\mathcal{M}_{12} = \frac{(-\lambda_3)^3}{(s-m_\chi^2)(t-m_\chi^2)}$
- $\mathcal{M}_{13} = \frac{(-\lambda_3)(-\lambda_4)}{t-m_\chi^2}$
- $\mathcal{M}_{14} = \frac{(-\lambda_3)(-\lambda_4)}{s-m_\chi^2}$
- $\mathcal{M}_{15t} = \frac{(-\lambda_3)^3}{(t-m_\chi^2)(t-m_\chi^2)}$
- $\mathcal{M}_{15u} = \frac{(-\lambda_3)^3}{(u-m_\chi^2)(t-m_\chi^2)}$
- $\mathcal{M}_{16t} = \frac{(-\lambda_3)(-\lambda_4)}{t-m_\chi^2}$
- $\mathcal{M}_{16u} = \frac{(-\lambda_3)(-\lambda_4)}{u-m_\chi^2}$

Only $h_{1,2}$ mediated,

- $\mathcal{M}_{1at} = \frac{(-\lambda_{a1})(-\lambda_{a2})}{t-m_{h_1}^2}$
- $\mathcal{M}_{1au} = \frac{(-\lambda_{a1})(-\lambda_{a2})}{u-m_{h_1}^2}$
- $\mathcal{M}_{2at} = \frac{(-\lambda_{a1})(-\lambda_{a2})}{t-m_{h_1}^2}$
- $\mathcal{M}_{2au} = \frac{(-\lambda_{a1})(-\lambda_{a2})}{u-m_{h_1}^2}$
- $\mathcal{M}_{3a} = \frac{(-\lambda_{a1})(-\lambda_{a2})}{t-m_{h_1}^2}$
- $\mathcal{M}_{1bt} = \frac{(-\lambda_{a1})(-\lambda_{a2})}{t-m_{h_2}^2}$
- $\mathcal{M}_{1bu} = \frac{(-\lambda_{a1})(-\lambda_{a2})}{u-m_{h_2}^2}$
- $\mathcal{M}_{2bt} = \frac{(-\lambda_{a1})(-\lambda_{a2})}{t-m_{h_2}^2}$
- $\mathcal{M}_{2bu} = \frac{(-\lambda_{a1})(-\lambda_{a2})}{u-m_{h_2}^2}$
- $\mathcal{M}_{3b} = \frac{(-\lambda_{a1})(-\lambda_{a2})}{t-m_{h_2}^2}$

h_1 and χ mediated

- $\mathcal{M}_{4at} = \frac{(-\lambda_{a1})^2(-\lambda_3)}{(t-m_{h_1}^2)(s-m_\chi^2)}$
- $\mathcal{M}_{4au} = \frac{(-\lambda_{a1})^2(-\lambda_3)}{(u-m_{h_1}^2)(s-m_\chi^2)}$
- $\mathcal{M}_{5at} = \frac{(-\lambda_{a1})^2(-\lambda_3)}{(s-m_{h_1}^2)(t-m_\chi^2)}$
- $\mathcal{M}_{5au} = \frac{(-\lambda_{a1})^2(-\lambda_3)}{(s-m_{h_1}^2)(-m_\chi^2)}$
- $\mathcal{M}_{6at} = \frac{(-\lambda_{a1})^2(-\lambda_3)}{(t-m_{h_1}^2)(s-m_\chi^2)}$
- $\mathcal{M}_{6au} = \frac{(-\lambda_{a1})^2(-\lambda_3)}{(u-m_{h_1}^2)(s-m_\chi^2)}$
- $\mathcal{M}_{7at} = \frac{(-\lambda_{a1})^2(-\lambda_3)}{(t-m_{h_1}^2)(t-m_\chi^2)}$
- $\mathcal{M}_{7au} = \frac{(-\lambda_{a1})^2(-\lambda_3)}{(s-m_{h_1}^2)(u-m_\chi^2)}$
- $\mathcal{M}_{8a} = \frac{(-\lambda_{a1})^2(-\lambda_3)}{(t-m_{h_1}^2)(s-m_\chi^2)}$
- $\mathcal{M}_{9at} = \frac{(-\lambda_{a1})^2(-\lambda_3)}{(t-m_{h_1}^2)(t-m_\chi^2)}$
- $\mathcal{M}_{9au} = \frac{(-\lambda_{a1})^2(-\lambda_3)}{(s-m_{h_1}^2)(u-m_\chi^2)}$
- $\mathcal{M}_{10at} = \frac{(-\lambda_{a1})^2(-\lambda_3)}{(s-m_{h_1}^2)(t-m_\chi^2)}$
- $\mathcal{M}_{10au} = \frac{(-\lambda_{a1})^2(-\lambda_3)}{(s-m_{h_1}^2)(u-m_\chi^2)}$

h_2 and χ mediated

- $\mathcal{M}_{4bt} = \frac{(-\lambda_{b1})^2(-\lambda_3)}{(t-m_{h_1}^2)(s-m_\chi^2)}$
- $\mathcal{M}_{4bu} = \frac{(-\lambda_{b1})^2(-\lambda_3)}{(u-m_{h_1}^2)(s-m_\chi^2)}$
- $\mathcal{M}_{5bt} = \frac{(-\lambda_{b1})^2(-\lambda_3)}{(s-m_{h_1}^2)(t-m_\chi^2)}$
- $\mathcal{M}_{5b} = \frac{(-\lambda_{b1})^2(-\lambda_3)}{(s-m_{h_1}^2)(u-m_\chi^2)}$
- $\mathcal{M}_{6bt} = \frac{(-\lambda_{b1})^2(-\lambda_3)}{(t-m_{h_1}^2)(s-m_\chi^2)}$
- $\mathcal{M}_{6bu} = \frac{(-\lambda_{b1})^2(-\lambda_3)}{(u-m_{h_1}^2)(s-m_\chi^2)}$
- $\mathcal{M}_{7bt} = \frac{(-\lambda_{b1})^2(-\lambda_3)}{(t-m_{h_1}^2)(t-m_\chi^2)}$
- $\mathcal{M}_{7bu} = \frac{(-\lambda_{b1})^2(-\lambda_3)}{(u-m_{h_1}^2)(t-m_\chi^2)}$
- $\mathcal{M}_{8b} = \frac{(-\lambda_{b1})^2(-\lambda_3)}{(t-m_{h_2}^2)(s-m_\chi^2)}$
- $\mathcal{M}_{9bt} = \frac{(-\lambda_{b1})^2(-\lambda_3)}{(t-m_{h_2}^2)(t-m_\chi^2)}$
- $\mathcal{M}_{9bu} = \frac{(-\lambda_{b1})^2(-\lambda_3)}{(u-m_{h_2}^2)(t-m_\chi^2)}$
- $\mathcal{M}_{10bt} = \frac{(-\lambda_{b1})^2(-\lambda_3)}{(s-m_{h_2}^2)(t-m_\chi^2)}$
- $\mathcal{M}_{10bt} = \frac{(-\lambda_{b1})^2(-\lambda_3)}{(s-m_{h_2}^2)(u-m_\chi^2)}$

$$
\begin{aligned}
\mathcal{M}_{net} =&(\mathcal{M}_{1at} + \mathcal{M}_{1au} + \mathcal{M}_{2at}\mathcal{M}_{2au} + \mathcal{M}_{3a} + \mathcal{M}_{4at} + \mathcal{M}_{4au} + \mathcal{M}_{5at} + \mathcal{M}_{5au} \\
&+ \mathcal{M}_{6at} + \mathcal{M}_{6au} + \mathcal{M}_{7at} + \mathcal{M}_{7au} + \mathcal{M}_{8a} + \mathcal{M}_{9at} + \mathcal{M}_{9au} + \mathcal{M}_{10at} + \mathcal{M}_{10au}) \\
&+ (\mathcal{M}_{1bt} + \mathcal{M}_{1bu} + \mathcal{M}_{2bt} + \mathcal{M}_{2bu} + \mathcal{M}_{3b} + \mathcal{M}_{4bt} + \mathcal{M}_{4bu} + \mathcal{M}_{5bt} + \mathcal{M}_{5bu} \\
&+ \mathcal{M}_{6bt} + \mathcal{M}_{6bu} + \mathcal{M}_{7bt} + \mathcal{M}_{7bu} + \mathcal{M}_{8b} + \mathcal{M}_{9bt} + \mathcal{M}_{9bu} + \mathcal{M}_{10bt} + \mathcal{M}_{10bu}) \\
&+ (\mathcal{M}_{11} + \mathcal{M}_{12} + \mathcal{M}_{13} + \mathcal{M}_{14} + \mathcal{M}_{15t} + \mathcal{M}_{15u} + \mathcal{M}_{16t} + \mathcal{M}_{16u})
\end{aligned}
$$

Note above that we have written the u-channel contribution also, which exists corresponding to each t-channel graph as the final state particles here are identical. Squared matrix amplitude is given as,

$$\Rightarrow |\mathcal{M}_{\chi\chi^*\chi^*\to\chi\chi}|^2 = \frac{1}{2}|\mathcal{M}_{Net}|^2$$

The complex conjugate of $\chi\chi^*\chi^* \to \chi\chi$ *i.e.* $\chi^*\chi\chi \to \chi^*\chi^*$ also contributes to the total matrix amplitude and has same expression as $\chi\chi^*\chi^* \to \chi\chi$,

$$|\mathcal{M}_{\chi\chi^*\chi^*\to\chi\chi}|^2 = |\mathcal{M}_{\chi^*\chi\chi\to\chi^*\chi^*}|^2$$

Therefore, the cross section for $3_{\rm DM} \to 2_{\rm DM}$ turns out to be:

$$\langle \sigma_{\chi\chi^*\chi^*\to\chi\chi} v^2 \rangle = \frac{\sqrt{5}}{192\pi m_\chi^3}\left[|\mathcal{M}_{\chi\chi^*\chi^*\to\chi\chi}|^2 + |\mathcal{M}_{\chi^*\chi\chi\to\chi^*\chi^*}|^2\right] = \frac{\sqrt{5}}{192\pi m_\chi^3}\left[2 * |\mathcal{M}_{\chi\chi^*\chi^*\to\chi\chi}|^2\right]$$

$$\begin{aligned}\langle \sigma_{3\to2} v^{2\rangle} &= \langle \sigma_{\chi\chi\chi\to\chi\chi^*} v^2\rangle + \langle \sigma_{\chi\chi^*\chi^*\to\chi\chi} v^2\rangle \\ &= \frac{\sqrt{5}}{192\pi m_\chi^3}\left[2 * \left(|\mathcal{M}_{\chi\chi\chi\to\chi\chi^*}|^2 + |\mathcal{M}_{\chi\chi^*\chi^*\to\chi\chi}|^2\right)\right] \end{aligned} \tag{B.2}$$

General expression for $3_{\rm DM} \to 2_{\rm DM}$ annihilation cross-section

Let us quickly derive the $3_{\rm DM} \to 2_{\rm DM}$ annihilation cross-section in a model independent way as a function of the amplitude. We are consider a process like:

$$\chi(p_1)\ \chi(p_2)\ \chi(p_3)\ \to\ \chi(p_4)\ \chi(p_5)$$

In Non-Relativistic limit,

$$\begin{aligned} E_1 = E_2 = E_3 &= m_\chi \\ \Rightarrow E_1 + E_2 + E_3 &= 3m_\chi \end{aligned} \tag{B.3}$$

where $P_{i=1-5}$ is the momentum of incoming and outgoing particles. Now, one can express the $(\sigma v^2)_{3_{DM}\to2_{DM}}$ as [24],

$$\begin{aligned}(\sigma v^2)_{3\to2} &= \frac{1}{(2E_1)(2E_2)(2E_3)}\int \frac{d^3P_4}{(2\pi)^3 2E_4}\frac{d^3P_5}{(2\pi)^3 2E_5}(2\pi)^4\delta^4(p_1+p_2+p_3-p_4-p_5)|\mathcal{M}|^2_{3\to2} \\ &= \frac{1}{(2E_1)(2E_2)(2E_3)}\frac{|\mathcal{M}|^2_{3\to2}}{(2\pi)^6}\int \frac{d^3P_4}{2E_4}\frac{d^3P_5}{2E_5}(2\pi)^4\delta(E_1+E_2+E_3-E_4-E_5) \quad \text{(B.4)} \\ &\qquad \delta^3(P_1+P_2+P_3-P_4-P_5) \quad \text{(B.5)}\end{aligned}$$

Assuming that the matrix amplitude is independent of the final outgoing particles. Now, in the center of mass frame $P_1 + P_2 + P_3 = 0$,

$$(\sigma v^2)_{3\to2} = \frac{1}{(2E_1)(2E_2)(2E_3)}\frac{|\mathcal{M}|^2_{3\to2}}{(2\pi)^2}\int \frac{d^3P_4}{2E_4}\frac{d^3P_5}{2E_5}\delta(E_1+E_2+E_3-E_4-E_5)\delta^3(P_4+P_5)$$

Using Eq.(B.3) and the delta function gives us $P_4 = -P_5$, we also know that $E_5 = \sqrt{P_5^2 + m_\chi^2}$. So, on integrating over P_5 we get,

$$\begin{aligned}(\sigma v^2)_{3\to2} &= \frac{1}{8m_\chi^3}\frac{|\mathcal{M}|^2_{3\to2}}{(2\pi)^2}\int \frac{d^3P_4}{2E_4}\frac{1}{2\sqrt{P_4+m_\chi^2}}\delta(3m_\chi - 2\sqrt{P_4^2+m_\chi^2}) \\ &= \frac{1}{8m_\chi^3}\frac{|\mathcal{M}|^2_{3\to2}}{(2\pi)^2}\int \frac{P_4^2 dP_4 d\Omega}{4(P_4+m_\chi^2)}\delta(3m_\chi - 2\sqrt{P_4^2+m_\chi^2}) \\ &= \frac{1}{8m_\chi^3}\frac{|\mathcal{M}|^2_{3\to2}}{(2\pi)^2}\frac{4\pi}{4}\int \frac{P_4^2 dP_4}{(P_4^2+m_\chi^2)}\delta(3m_\chi - 2\sqrt{P_4^2+m_\chi^2}) \\ &= \frac{1}{8m_\chi^3}\frac{|\mathcal{M}|^2_{3\to2}}{4\pi}\int \frac{P_4^2 dP_4}{(P_4+m_\chi^2)}\delta(3m_\chi - 2\sqrt{P_4^2+m_\chi^2}) \\ &= \frac{1}{2\times 32\pi m_\chi^3}|\mathcal{M}|^2_{3\to2}\int \frac{P_4^2 dP_4}{(P_4+m_\chi^2)}\delta(\frac{3}{2}m_\chi - \sqrt{P_4^2+m_\chi^2})\end{aligned}$$

Now, integrating over P_4 we get,

$$(\sigma v^2)_{3\to 2} = \frac{\sqrt{5}}{3} \times \frac{1}{64\pi m_\chi^3} |\mathcal{M}|^2_{3\to 2} \tag{B.6}$$

The thermal averaged cross section under the conditions mentioned above can be written as,

$$\langle \sigma v^2 \rangle_{3\to 2} = \frac{1}{n_1^{eq}\ n_2^{eq}\ n_3^{eq}} \int \frac{g_{DM}\ d^3P_1}{(2\pi)^3 2E_1} \frac{g_{DM}\ d^3P_2}{(2\pi)^3 2E_2} \frac{g_{DM}\ d^3P_3}{(2\pi)^3 2E_3} \frac{g_{DM}\ d^3P_4}{(2\pi)^3 2E_4} \frac{g_{DM}\ d^3P_5}{(2\pi)^3 2E_5}$$
$$(2\pi)^4 \delta^4(p_1 + p_2 + p_3 - p_4 - p_5) \times |\mathcal{M}_{3\to 2}|^2\ f_1^{eq} f_2^{eq} f_3^{eq} \tag{B.7}$$

Using Eq.(**??**) and Eq.(B.7), we can write,

$$\langle \sigma v^2 \rangle_{3\to 2} = \frac{1}{n_1^{eq}\ n_2^{eq}\ n_3^{eq}} \int \frac{g_{DM}\ d^3P_1}{(2\pi)^3} \frac{g_{DM}\ d^3P_2}{(2\pi)^3} \frac{g_{DM}\ d^3P_3}{(2\pi)^3}\ f_1^{eq} f_2^{eq} f_3^{eq}\ (\sigma v^2)_{3\to 2} \tag{B.8}$$

Where n_i^{eq} can be expressed in terms of modified Bessel's function as [20],

$$n_i^{eq} = \frac{g_{DM}}{(2\pi)^3} \int d^3P\ f^{eq}(E_i, T) \tag{B.9}$$

Since,

$$d^3P_i\ f^{eq}(E_i,T) = 4\pi m_\chi^3 \left(\frac{E_i}{m_\chi}\right) \left(\sqrt{\left(\frac{E_i}{m_\chi}\right)^2 - 1}\right) e^{-(\frac{E_i}{m_\chi})(\frac{m_\chi}{T})} d\left(\frac{E_i}{m_\chi}\right)$$
$$\int d^3P_i\ f^{eq}(E_i,T) = 4\pi m_\chi^3 \int \left(\frac{E_i}{m_\chi}\right) \left(\sqrt{\left(\frac{E_i}{m_\chi}\right)^2 - 1}\right) e^{-(\frac{E_i}{m_\chi})(\frac{m_\chi}{T})} d\left(\frac{E_i}{m_\chi}\right)$$
$$= 4\pi m_\chi^3 \frac{K_2(m_\chi/T)}{m_\chi/T} = 4\pi m_\chi^2 T K_2(m_\chi/T) \tag{B.10}$$

So,

$$n_i^{eq} = \frac{g_{DM}}{(2\pi)^3}\ 4\pi m_\chi^2 T K_2(m_\chi/T) \tag{B.11}$$

Now one can write the $\langle \sigma v^2 \rangle_{3\to 2}$ as follows:

$$\Rightarrow \langle \sigma v^2 \rangle_{3\to 2} = \frac{1}{(4\pi m_\chi^2 T K_2(m_\chi/T))^3} \int (\sigma v^2)_{3\to 2}\ f_1^{eq}\ f_2^{eq}\ f_3^{eq} d^3P_1\ d^3P_2\ d^3P_3$$

$$\Rightarrow \langle \sigma v^2 \rangle_{3\to 2} = \frac{1}{(4\pi m_\chi^2 T K_2(m_\chi/T))^3} \int \frac{\sqrt{5}}{192\pi E_1\ E_2\ E_3} |\mathcal{M}|^2_{3\to 2}$$
$$\left[4\pi m_\chi^3 \left(\frac{E_1}{m_\chi}\right) \left(\sqrt{\left(\frac{E_1}{m_\chi}\right)^2 - 1}\right) e^{-(\frac{E_1}{m_\chi})(\frac{m_\chi}{T})} d\left(\frac{E_1}{m_\chi}\right)\right]$$
$$\left[4\pi m_\chi^3 \left(\frac{E_2}{m_\chi}\right) \left(\sqrt{\left(\frac{E_2}{m_\chi}\right)^2 - 1}\right) e^{-(\frac{E_2}{m_\chi})(\frac{m_\chi}{T})} d\left(\frac{E_2}{m_\chi}\right)\right]$$
$$\left[4\pi m_\chi^3 \left(\frac{E_3}{m_\chi}\right) \left(\sqrt{\left(\frac{E_3}{m_\chi}\right)^2 - 1}\right) e^{-(\frac{E_3}{m_\chi})(\frac{m_\chi}{T})} d\left(\frac{E_3}{m_\chi}\right)\right] \tag{B.12}$$

$$
\begin{aligned}
\Rightarrow \langle \sigma v^2 \rangle_{3\to 2} &= \frac{1}{(4\pi m_\chi^2 T K_2(m_\chi/T))^3}\ (4\pi m_\chi^2)^3\ \frac{\sqrt{5}}{192\pi}|\mathcal{M}|^2_{3\to 2} \\
&\int \Bigg[\left(\sqrt{\left(\frac{E_1}{m_\chi}\right)^2 - 1}\right) e^{-(\frac{E_1}{m_\chi})(\frac{m_\chi}{T})} d\left(\frac{E_1}{m\chi}\right)\Bigg] \\
&\Bigg[\left(\sqrt{\left(\frac{E_2}{m_\chi}\right)^2 - 1}\right) e^{-(\frac{E_2}{m_\chi})(\frac{m_\chi}{T})} d\left(\frac{E_2}{m_\chi}\right)\Bigg] \\
&\Bigg[\left(\sqrt{\left(\frac{E_3}{m_\chi}\right)^2 - 1}\right) e^{-(\frac{E_3}{m_\chi})(\frac{m_\chi}{T})} d\left(\frac{E_3}{m_\chi}\right)\Bigg] \\
&= \frac{1}{(4\pi m_\chi^2 T K_2(m_\chi/T))^3}\ (4\pi m_\chi^2)^3\ \frac{\sqrt{5}}{192\pi}|\mathcal{M}|^2_{3\to 2}\left(\frac{K_1(m_\chi/T)}{m_\chi/T}\right)^3 \\
&= \left(\frac{K_1(m_\chi/T)}{K_2(m_\chi/T)}\right)^3 \frac{\sqrt{5}}{192\pi m_\chi^3}|\mathcal{M}|^2_{3\to 2} \\
&\approx \frac{\sqrt{5}}{192\pi m_\chi^3}|\mathcal{M}|^2_{3\to 2} \qquad \text{(B.13)}
\end{aligned}
$$

C Self Scattering cross-section of DM

We consider here all the processes that yield self scattering. There are two processes in the model essentially: $\chi\chi \to \chi\chi$ and $\chi\chi^* \to \chi\chi^*$ and their conjugates.

$$\underline{\chi\chi \to \chi\chi}$$

Feynman Diagrams

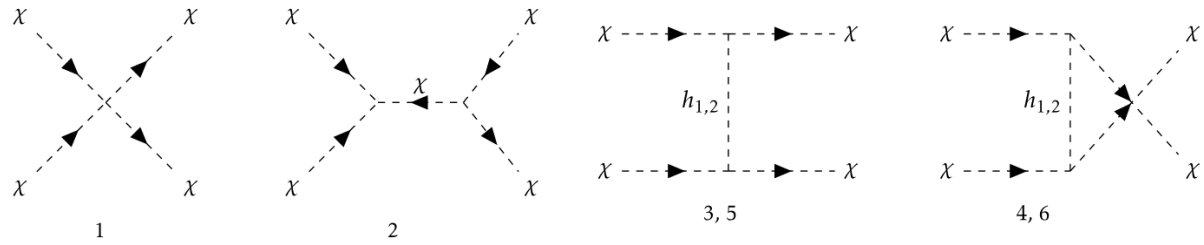

Matrix Amplitude

$$\mathcal{M}_1 = -4\lambda_\chi$$

$$\mathcal{M}_2 = \frac{[-(\mu_\chi + Y_{\chi\phi} v_\phi)]^2}{s - m_\chi^2}$$

$$\mathcal{M}_3 = \frac{[-(\lambda_{\chi h} v_h \cos\theta - (\lambda_{\chi\phi} v_\phi + \mu_{\chi\phi})\sin\theta)]^2}{t - m_{h_1}^2}$$

$$\mathcal{M}_4 = \frac{[-(\lambda_{\chi h} v_h \cos\theta - (\lambda_{\chi\phi} v_\phi + \mu_{\chi\phi})\sin\theta)]^2}{u - m_{h_1}^2}$$

$$\mathcal{M}_5 = \frac{[-(\lambda_{\chi h} v_h \sin\theta + (\lambda_{\chi\phi} v_\phi + \mu_{\chi\phi})\cos\theta)]^2}{t - m_{h_2}^2}$$

$$\mathcal{M}_6 = \frac{[-(\lambda_{\chi h} v_h \sin\theta + (\lambda_{\chi\phi} v_\phi + \mu_{\chi\phi})\cos\theta)]^2}{u - m_{h_2}^2}$$

Net Matrix amplitude for $\chi\chi \to \chi\chi$ is,

$$\mathcal{M}_{Net} = \mathcal{M}_1 + \mathcal{M}_2 + \mathcal{M}_3 + \mathcal{M}_4 + \mathcal{M}_5 + \mathcal{M}_6$$

Squared matrix amplitude is given as,

$$\Rightarrow |\mathcal{M}_{\chi\chi\to\chi\chi}|^2 = \frac{1}{2}|\mathcal{M}_{Net}|^2$$

The complex conjugate of $\chi\chi \to \chi\chi$ *i.e.* $\chi^*\chi^* \to \chi^*\chi^*$ also contributes to the total matrix amplitude and has same expression as $\chi\chi \to \chi\chi$,

$$|\mathcal{M}_{\chi\chi\to\chi\chi}|^2 = |\mathcal{M}_{\chi^*\chi^*\to\chi^*\chi^*}|^2$$

The cross section turns out to be

$$\begin{aligned}\sigma_{\chi\chi\to\chi\chi} &= \frac{1}{64\pi m_\chi^2}\left[|\mathcal{M}_{\chi\chi\to\chi\chi}|^2 + |\mathcal{M}_{\chi^*\chi^*\to\chi^*\chi^*}|^2\right] \\ &= \frac{1}{64\pi m_\chi^2}\left[2 * |\mathcal{M}_{\chi\chi\to\chi\chi}|^2\right]. \end{aligned} \tag{C.1}$$

$\underline{\chi\chi^* \to \chi\chi^*}$

Feynman diagrams

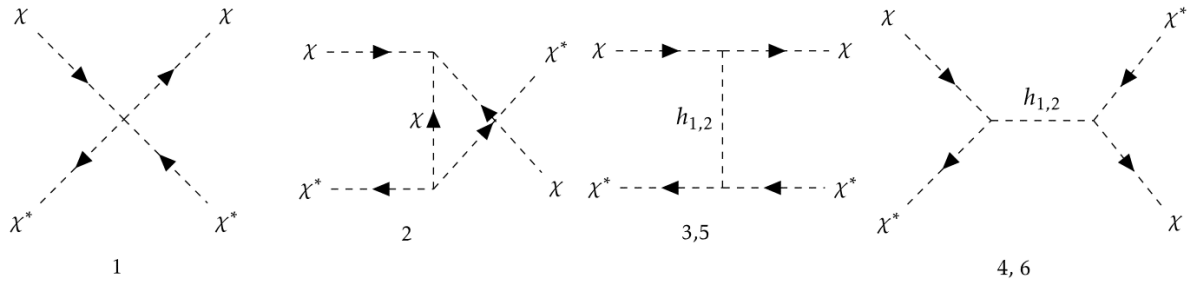

Matrix Amplitude

$$\mathcal{M}_1 = -4\lambda_\chi$$

$$\mathcal{M}_2 = \frac{[-(\mu_\chi + Y_{\chi\phi} v_\phi)]^2}{u - m_\chi^2}$$

$$\mathcal{M}_3 = \frac{[-(\lambda_{\chi h} v_h Cos\theta - (\lambda_{\chi\phi} v_\phi + \mu_{\chi\phi})Sin\theta)]^2}{t - m_{h_1}^2}$$

$$\mathcal{M}_4 = \frac{[-(\lambda_{\chi h} v_h Cos\theta - (\lambda_{\chi\phi} v_\phi + \mu_{\chi\phi})Sin\theta)]^2}{s - m_{h_1}^2}$$

$$\mathcal{M}_5 = \frac{[-(\lambda_{\chi h} v_h Sin\theta + (\lambda_{\chi\phi} v_\phi + \mu_{\chi\phi}) Cos\theta)]^2}{t - m_{h_2}^2}$$

$$\mathcal{M}_6 = \frac{[-(\lambda_{\chi h} v_h Sin\theta + (\lambda_{\chi\phi} v_\phi + \mu_{\chi\phi}) Cos\theta)]^2}{s - m_{h_2}^2}$$

Net Matrix amplitude for $\chi\chi^* \to \chi\chi^*$ is,

$$\mathcal{M}_{Net} = \mathcal{M}_1 + \mathcal{M}_2 + \mathcal{M}_3 + \mathcal{M}_4 + \mathcal{M}_5 + \mathcal{M}_6$$

Squared matrix amplitude is given as,

$$\Rightarrow |\mathcal{M}_{\chi\chi^* \to \chi\chi^*}|^2 = |\mathcal{M}_{Net}|^2$$

The complex conjugate of $\chi\chi^* \to \chi\chi^*$ *i.e.* $\chi^*\chi \to \chi^*\chi$ also contributes to the total matrix amplitude and has same expression as $\chi\chi^* \to \chi\chi^*$,

$$|\mathcal{M}_{\chi\chi^* \to \chi\chi^*}|^2 = |\mathcal{M}_{\chi^*\chi \to \chi^*\chi}|^2$$

The Cross section for this process then turns out to be

$$\sigma_{\chi\chi^* \to \chi\chi^*} = \frac{1}{64\pi m_\chi^2} \left[|\mathcal{M}_{\chi\chi^* \to \chi\chi^*}|^2 \right]$$

Finally, adding both contributions, the total scattering cross-section is

$$\begin{aligned} \sigma_{self} &= 2 * (\sigma_{\chi\chi \to \chi\chi} + \sigma_{\chi\chi^* \to \chi\chi^*}) \\ &= \frac{1}{64\pi m_\chi^2} \left[2 * \left(|\mathcal{M}_{\chi\chi \to \chi\chi}|^2 + |\mathcal{M}_{\chi\chi^* \to \chi\chi^*}|^2 \right) \right] \end{aligned}$$

D Annihilation cross-section to SM

$$\underline{\chi(p_1)\chi(p_2)\chi(p_3) \to f(k_1)\bar{f}(k_2)}$$

Feynman Diagrams

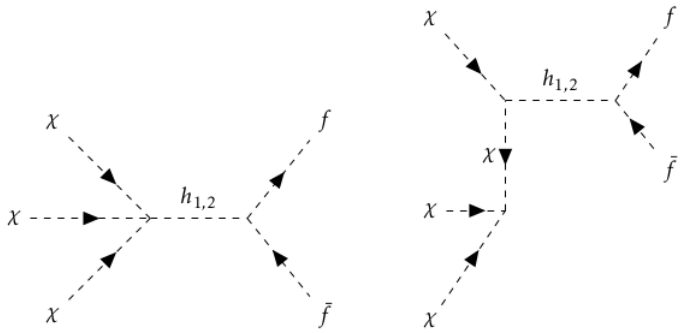

We will focus on two types of annihilations here: $3 \to 2$ and $2 \to 2$. The former is not discussed in details and therefore we will first analyse the processes that contribute to $3 \to 2$ annihilation in this model and also compute the generic form of such cross-section.

Matrix Amplitude

$$|\mathcal{M}_{\chi\chi\chi\to f\bar{f}}|^2 = 2(s-4m_f^2)\left[\frac{\lambda_{a2}\lambda_{f1}}{s-m_{h_1}^2}+\frac{\lambda_{b2}\lambda_{f2}}{s-m_{h_2}^2}+\frac{\lambda_3\lambda_{a1}\lambda_{f1}}{(s-m_{h_1}^2)(t-m_\chi^2)}+\frac{\lambda_3\lambda_{b1}\lambda_{f2}}{(s-m_{h_2}^2)(t-m_\chi^2)}\right]^2$$

The complex conjugate of $\chi\chi\chi \to f\bar{f}$ *i.e.* $\chi^*\chi^*\chi^* \to \bar{f}f$also contributes to the total matrix amplitude and has same expression as $\chi\chi\chi \to f\bar{f}$,

$$|\mathcal{M}_{\chi\chi\chi\to f\bar{f}}|^2 = |\mathcal{M}_{\chi^*\chi^*\chi^*\to \bar{f}f}|^2$$

Therefore the cross-section for $3 \to 2$ in SM is :

$$\langle\sigma v\rangle_{\chi\chi\chi\to f\bar{f}} = \frac{1}{64\pi m_\chi^3}\left(1-\frac{4m_f^2}{9m_\chi^2}\right)^{1/2}\left[|\mathcal{M}_{\chi\chi\chi\to f\bar{f}}|^2+|\mathcal{M}_{\chi^*\chi^*\chi^*\to \bar{f}f}|^2\right]$$

$$\langle\sigma v\rangle_{\chi\chi\chi\to f\bar{f}} = \frac{1}{64\pi m_\chi^3}\left(1-\frac{4m_f^2}{9m_\chi^2}\right)^{1/2}\left[2*|\mathcal{M}_{\chi\chi\chi\to f\bar{f}}|^2\right] \tag{D.1}$$

General expression for $3_{\mathrm{DM}} \to 2_{\mathrm{SM}}$ annihilation cross-section

Let us quickly derive the $3_{\mathrm{DM}} \to 2_{\mathrm{SM}}$ annihilation cross-section in a model independent way as a function of the amplitude. We are consider a process like:

$$\chi(p_1)\ \chi(p_2)\ \chi(p_3)\ \to\ f(p_4)\ f(p_5)$$

Following a similar procedure that we adopted for $3_{DM} \to 2_{DM}$ annihilation crossection we can derive an expression for $3_{DM} \to 2_{DM}$ as follows,

$$\begin{aligned}
(\sigma v^2)_{3\to2} &= \frac{1}{8m_\chi^3}\frac{|\mathcal{M}|^2_{3\to2}}{(2\pi)^2}\int\frac{d^3P_4}{2E_4}\frac{1}{2\sqrt{P_4+m_f^2}}\delta(3m_\chi-2\sqrt{P_4^2+m_f^2}) \\
&= \frac{1}{8m_\chi^3}\frac{|\mathcal{M}|^2_{3\to2}}{(2\pi)^2}\int\frac{P_4^2dP_4d\Omega}{4(P_4+m_f^2)}\delta(3m_\chi-2\sqrt{P_4^2+m_f^2}) \\
&= \frac{1}{8m_\chi^3}\frac{|\mathcal{M}|^2_{3\to2}}{(2\pi)^2}\frac{4\pi}{4}\int\frac{P_4^2dP_4}{(P_4^2+m_f^2)}\delta(3m_\chi-2\sqrt{P_4^2+m_f^2}) \\
&= \frac{1}{8m_\chi^3}\frac{|\mathcal{M}|^2_{3\to2}}{4\pi}\int\frac{P_4^2dP_4}{(P_4+m_f^2)}\delta(3m_\chi-2\sqrt{P_4^2+m_f^2}) \\
&= \frac{1}{2\times32\pi m_\chi^3}|\mathcal{M}|^2_{3\to2}\int\frac{P_4^2dP_4}{(P_4+m_f^2)}\delta(\frac{3}{2}m_\chi-\sqrt{P_4^2+m_f^2})
\end{aligned}$$

Now, integrating over P_4 we get,

$$(\sigma v^2)_{3\to2} = \frac{1}{64\pi m_\chi^3}\left(1-\frac{4m_f^2}{9m_\chi^2}\right)^{1/2}|\mathcal{M}|^2_{3_{DM}\to2_{SM}} \tag{D.2}$$

We can write the thermally averaged crossection for $3_{DM} \to 2_{SM}$ just like we did for $3_{DM} \to 2_{SM}$ in B.7. So, we can write the thermally averaged $3_{DM} \to 2_{SM}$ crossection as,

$$\langle\sigma v^2\rangle_{3\to2} = \frac{1}{64\pi m_\chi^3}\left(1-\frac{4m_f^2}{9m_\chi^2}\right)^{1/2}|\mathcal{M}|^2_{3_{DM}\to2_{SM}} \tag{D.3}$$

$$\underline{\chi(p_1)\chi^*(p_2) \to f(k_1)\bar{f}(k_2)}$$

Feynman Diagrams

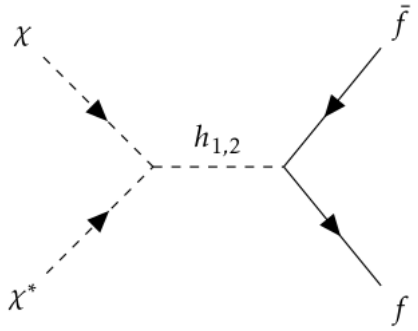

Matrix Amplitude

$$\mathcal{M}_1 = \lambda_{a_1} \frac{1}{s - m_{h_1}^2} \bar{u}(k_1) \lambda_{f_1} v(k_2)$$

$$\mathcal{M}_2 = \lambda_{b_1} \frac{1}{s - m_{h_2}^2} \bar{u}(k_1) \lambda_{f_2} v(k_2)$$

Net Matrix amplitude for $\chi\chi^* \to f\bar{f}$ is,

$$\mathcal{M}_{Net} = \mathcal{M}_1 + \mathcal{M}_2$$

Squared matrix amplitude is given as,

$$\Rightarrow |\mathcal{M}_{\chi\chi^* \to f\bar{f}}|^2 = |\mathcal{M}_{Net}|^2$$

$$|\mathcal{M}_{\chi\chi^* \to f\bar{f}}|^2 = 2 \times 2(s - 4m_f^2) \left(\frac{\lambda_{a1}\lambda_{f_1}}{(s - m_{h_1}^2)^2} + \frac{\lambda_{b1}\lambda_{f_2}}{(s - m_{h_2}^2)^2} \right)^2 . \tag{D.4}$$

The complex conjugate of $\chi\chi^* \to f\bar{f}$ *i.e.* $\chi^*\chi \to \bar{f}f$also contributes to the total matrix amplitude and has same expression as $\chi\chi^* \to f\bar{f}$,

$$|\mathcal{M}_{\chi\chi^* \to f\bar{f}}|^2 = |\mathcal{M}_{\chi^*\chi \to \bar{f}f}|^2$$

Therefore, the cross section is

$$\begin{aligned} \langle \sigma v \rangle_{\chi\chi^* \to f\ \bar{f}} &= \frac{1}{32\pi m_\chi^2} \left[|\mathcal{M}_{\chi\chi^* \to f\bar{f}}|^2 + |\mathcal{M}_{\chi^*\chi \to \bar{f}f}|^2 \right] \\ &= \frac{1}{32\pi m_\chi^2} \left[2 * |\mathcal{M}_{\chi\chi^* \to f\bar{f}}|^2 \right] \end{aligned} \tag{D.5}$$

E Scattering cross-section of DM with SM

We compute the scattering cross-section for the DM with SM fermions. This is required for analysing the kinetic equilibrium of the DM in early universe as well as for the direct search prospects of the DM.

$$\underline{\chi(p_1)f(k_1) \to \chi(p_2)f(k_2)}$$

Feynman Diagrams

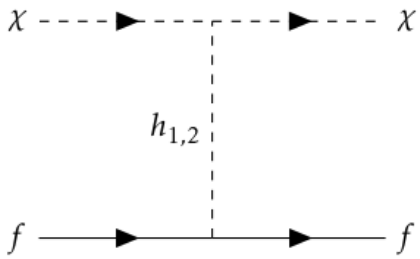

Matrix Amplitude

$$\mathcal{M}_1 = \lambda_{a_1} \frac{1}{t - m_{h_1}^2} \bar{u}(k_1)\lambda_{f_1} v(k_2)$$

$$\mathcal{M}_2 = \lambda_{b_1} \frac{1}{t - m_{h_2}^2} \bar{u}(k_1)\lambda_{f_2} v(k_2)$$

Net Matrix amplitude for $\chi f \to \chi f$ is,

$$\mathcal{M}_{Net} = \mathcal{M}_1 + \mathcal{M}_2$$

Squared matrix amplitude is given as,

$$\Rightarrow |\mathcal{M}_{\chi f \to \chi f}|^2 = |\mathcal{M}_{Net}|^2$$

$$|\mathcal{M}_{\chi f \to \chi f}|^2 = 2 \times (-2)(t - 4m_f^2)\left(\frac{\lambda_{a1}\lambda_{f_1}}{(t - m_{h_1}^2)^2} + \frac{\lambda_{b1}\lambda_{f_2}}{(t - m_{h_2}^2)^2}\right)^2 . \tag{E.1}$$

The complex conjugate of $\chi f \to \chi f$ *i.e.* $\chi^*\chi^* \to \bar{f}\bar{f}$also contributes to the total matrix amplitude and has same expression as $\chi f \to \chi f$,

$$|\mathcal{M}_{\chi f \to \chi f}|^2 = |\mathcal{M}_{\chi^*\chi^* \to \bar{f}\bar{f}}|^2$$

Therefore the cross-section for $2 \to 2$ scattering turns out to be:

$$\begin{aligned} \langle \sigma v \rangle_{\chi f \to \chi f} &= \frac{1}{16\pi m_\chi^2}\left[|\mathcal{M}_{\chi f \to \chi f}|^2 + |\mathcal{M}_{\chi^*\chi^* \to \bar{f}\bar{f}}|^2\right] \\ &= \frac{1}{16\pi m_\chi^2}\left[2 * |\mathcal{M}_{\chi f \to \chi f}|^2\right] \end{aligned} \tag{E.2}$$

References

[1] V. C. Rubin, *Optical observations of radio galaxies and quasi-stellar objectsOptical observations of radio galaxies and quasi-stellar radiosources*, in *Hautes Energies en Astrophysique: Proceedings, Ecole d'Et de Physique Thorique, Les Houches, France, 1966, vol. 1*, pp. 133–152, 1967.

[2] V. C. Rubin and W. K. Ford, Jr., *Rotation of the Andromeda Nebula from a Spectroscopic Survey of Emission Regions*, *Astrophys. J.* **159** (1970) 379–403.

[3] G. Bertone, D. Hooper and J. Silk, *Particle dark matter: Evidence, candidates and constraints*, *Phys. Rept.* **405** (2005) 279–390, [hep-ph/0404175].

[4] W. Hu and S. Dodelson, *Cosmic microwave background anisotropies*, *Ann. Rev. Astron. Astrophys.* **40** (2002) 171–216, [astro-ph/0110414].

[5] WMAP collaboration, G. Hinshaw et al., *Nine-Year Wilkinson Microwave Anisotropy Probe (WMAP) Observations: Cosmological Parameter Results*, *Astrophys. J. Suppl.* **208** (2013) 19, [1212.5226].

[6] XENON collaboration, E. Aprile et al., *Dark Matter Search Results from a One Ton-Year Exposure of XENON1T*, *Phys. Rev. Lett.* **121** (2018) 111302, [1805.12562].

[7] LUX collaboration, D. S. Akerib et al., *Limits on spin-dependent WIMP-nucleon cross section obtained from the complete LUX exposure*, *Phys. Rev. Lett.* **118** (2017) 251302, [1705.03380].

[8] MAGIC, Fermi-LAT collaboration, M. L. Ahnen et al., *Limits to Dark Matter Annihilation Cross-Section from a Combined Analysis of MAGIC and Fermi-LAT Observations of Dwarf Satellite Galaxies*, *JCAP* **1602** (2016) 039, [1601.06590].

[9] D. Abercrombie et al., *Dark Matter Benchmark Models for Early LHC Run-2 Searches: Report of the ATLAS/CMS Dark Matter Forum*, 1507.00966.

[10] E. W. Kolb and M. S. Turner, *The Early Universe*, *Front. Phys.* **69** (1990) 1–547.

[11] Planck collaboration, P. A. R. Ade et al., *Planck 2015 results. XIII. Cosmological parameters*, *Astron. Astrophys.* **594** (2016) A13, [1502.01589].

[12] S. Bhattacharya, P. Ghosh, T. N. Maity and T. S. Ray, *Mitigating Direct Detection Bounds in Non-minimal Higgs Portal Scalar Dark Matter Models*, *JHEP* **10** (2017) 088, [1706.04699].

[13] S. Bhattacharya, P. Ghosh and N. Sahu, *Multipartite Dark Matter with Scalars, Fermions and signatures at LHC*, *JHEP* **02** (2019) 059, [1809.07474].

[14] Y. Hochberg, E. Kuflik, T. Volan sky and J. G. Wacker, *Mechanism for thermal relic dark matter of strongly interacting massive particles*, *Phys. Rev. Lett.* **113** (Oct, 2014) 171301.

[15] S. W. Randall, M. Markevitch, D. Clowe, A. H. Gonzalez and M. Bradac, *Constraints on the Self-Interaction Cross-Section of Dark Matter from Numerical Simulations of the Merging Galaxy Cluster 1E 0657-56*, *Astrophys. J.* **679** (2008) 1173–1180, [0704.0261].

[16] F. Kahlhoefer, K. Schmidt-Hoberg, J. Kummer and S. Sarkar, *On the interpretation of dark matter self-interactions in Abell 3827*, *Mon. Not. Roy. Astron. Soc.* **452** (2015) L54–L58, [1504.06576].

[17] W. J. G. de Blok, *The Core-Cusp Problem*, *Adv. Astron.* **2010** (2010) 789293, [0910.3538].

[18] M. Boylan-Kolchin, J. S. Bullock and M. Kaplinghat, *Too big to fail? The puzzling darkness of massive Milky Way subhaloes*, *Mon. Not. Roy. Astron. Soc.* **415** (2011) L40, [1103.0007].

[19] S.-M. Choi and H. M. Lee, *SIMP dark matter with gauged Z_3 symmetry*, *JHEP* **09** (2015) 063, [1505.00960].

[20] L. Feng, S. Profumo and L. Ubaldi, *Closing in on singlet scalar dark matter: LUX, invisible Higgs decays and gamma-ray lines*, *JHEP* **03** (2015) 045, [1412.1105].

[21] S. Bhattacharya, P. Poulose and P. Ghosh, *Multipartite Interacting Scalar Dark Matter in the light of updated LUX data*, *JCAP* **1704** (2017) 043, [1607.08461].

[22] E. Kuflik, M. Perelstein, N. R.-L. Lorier and Y.-D. Tsai, *Elastically Decoupling Dark Matter*, *Phys. Rev. Lett.* **116** (2016) 221302, [1512.04545].

[23] U. K. Dey, T. N. Maity and T. S. Ray, *Light Dark Matter through Assisted Annihilation*, *JCAP* **1703** (2017) 045, [1612.09074].

[24] M. Pierre, *Dark Matter phenomenology : from simplified WIMP models to refined alternative solutions*. PhD thesis, Orsay, LPT, 2018. 1901.05822.

[25] S. C. Mancas and H. C. Rosu, *Integrable abel equations and vein's abel equation*, *Mathematical Methods in the Applied Sciences* **39** (2016) 1376–1387, [https://onlinelibrary.wiley.com/doi/pdf/10.1002/mma.3575].

[26] Y. Hochberg, E. Kuflik, H. Murayama, T. Volansky and J. G. Wacker, *Model for Thermal Relic Dark Matter of Strongly Interacting Massive Particles*, *Phys. Rev. Lett.* **115** (2015) 021301, [1411.3727].

[27] P. Ko and Y. Tang, *Self-interacting scalar dark matter with local Z_3 symmetry*, *JCAP* **1405** (2014) 047, [1402.6449].

[28] S.-M. Choi, Y. Hochberg, E. Kuflik, H. M. Lee, Y. Mambrini, H. Murayama et al., *Vector SIMP dark matter*, *JHEP* **10** (2017) 162, [1707.01434].

[29] S.-M. Choi, H. M. Lee, P. Ko and A. Natale, *Unitarizing SIMP scenario with dark vector resonances*, in *39th International Conference on High Energy Physics (ICHEP 2018) Seoul, Gangnam-Gu, Korea, Republic of, July 4-11, 2018*, 2018. 1811.02751.

[30] S.-M. Choi, Y.-J. Kang and H. M. Lee, *On thermal production of self-interacting dark matter*, *JHEP* **12** (2016) 099, [1610.04748].

[31] S.-M. Choi, H. M. Lee and M.-S. Seo, *Cosmic abundances of SIMP dark matter*, *JHEP* **04** (2017) 154, [1702.07860].

[32] A. Beniwal, M. Lewicki, M. White and A. G. Williams, *Gravitational waves and electroweak baryogenesis in a global study of the extended scalar singlet model*, *JHEP* **02** (2019) 183, [1810.02380].

[33] S. Bhattacharya, I. de Medeiros Varzielas, B. Karmakar, S. F. King and A. Sil, *Dark side of the Seesaw*, 1806.00490.

[34] P. Ghosh, A. K. Saha and A. Sil, *Study of Electroweak Vacuum Stability from Extended Higgs Portal of Dark Matter and Neutrinos*, *Phys. Rev.* **D97** (2018) 075034, [1706.04931].

[35] A. Semenov, *LanHEP: A Package for the automatic generation of Feynman rules in field theory. Version 3.0*, *Comput. Phys. Commun.* **180** (2009) 431–454, [0805.0555].

[36] A. Belyaev, N. D. Christensen and A. Pukhov, *CalcHEP 3.4 for collider physics within and beyond the standard model*, *Computer Physics Communications* **184** (jul, 2013) 1729–1769.

[37] M. Dohse, *TikZ-FeynHand: Basic User Guide*, 1802.00689.

[38] Wolfram Research Inc., *Mathematica 10.0*, 2014.

[39] M. E. Peskin and D. V. Schroeder, *An Introduction to quantum field theory*. Addison-Wesley, Reading, USA, 1995.

[40] G. Belanger, F. Boudjema and A. Pukhov, *micrOMEGAs : a code for the calculation of Dark Matter properties in generic models of particle interaction*, in *The Dark Secrets of the Terascale: Proceedings, TASI 2011, Boulder, Colorado, USA, Jun 6 - Jul 11, 2011*, pp. 739–790, 2013. 1402.0787. DOI.